J. Fluid Mech. (1991), *vol.* 227, *pp.* 161–192
Printed in Great Britain

Faraday resonance in rectangular geometry

By MAKOTO UMEKI
Department of Physics, University of Tokyo, Hongo, Bunkyo-ku, Tokyo 113, Japan

(Received 18 April 1989 and in revised form 28 November 1990)

The motion of subharmonic resonant modes of surface waves in a rectangular container subjected to vertical periodic oscillation is studied based on the weakly nonlinear model equations derived by both the average Lagrangian and the two-timescale method. Explicit estimates of the nonlinearity of some specific modes are given. The bifurcations of stationary states including a Hopf bifurcation are examined. Numerical calculations of the dissipative dynamical equations show periodic and chaotic attractors. Theoretical parameter-space diagrams and numerical results are compared in detail with Simonelli & Gollub's (1989) surface-wave mode-competition experiments. It is shown that the average Hamiltonian system for the present 2:1 : 1 external–internal resonance with suitable coefficients has homoclinic chaos, which was mathematically proven by Holmes (1986) for the specific case of 2:1:2 external–internal resonance.

1. Introduction

Chaotic mode competition of parametrically excited surface waves has been attracting much theoretical and experimental attention. Ciliberto & Gollub (1985) studied experimentally the temporal evolution of two internal resonant modes, (4, 3) and (7, 2) (eigenmode indices), in a circular cylindrical container and revealed a parameter region where periodic and chaotic mode (eigenmode) competition occurs. A more sophisticated experiment that included the bifurcation and hysteresis phenomena was done by Simonelli & Gollub (1989, hereinafter referred to as SG 1989), who investigated the dynamics of two resonant modes, (3, 2) and (2, 3), in a square and slightly rectangular container.

Benjamin & Ursell (1954) showed that the linear problem of the parametric excitation is equivalent to the Mathieu's equation of each mode, thus causing theoretical interest to be focused on the evaluation of the nonlinearity. Two- and three-dimensional, spatially periodic gravity waves were analysed for a single mode by Tadjbakhsh & Keller (1960) and Verma & Keller (1962). An axisymmetric mode and two completely degenerate antisymmetric modes of gravity waves in a circular cylindrical container were respectively studied by Mack (1962) and Miles (1984*b*). The above studies used a perturbation expansion method, except for Miles (1984*b*) who invoked an average Lagrangian method.

Meron & Procaccia (1987) analysed the experiment of Ciliberto & Gollub (1985) and used the normal-form transformations to derive associated dynamical equations. They expressed the coefficients of nonlinear terms in terms of correlation integrals, yet did not evaluate them. Miles (1989) pointed out that Meron & Procaccia (1986) resulting equations do not lead to the canonical formulations. A re-examination of Ciliberto & Gollub (1985) was done by Umeki & Kambe (1989) using an extension of Miles's formulation. The original four-degree-of-freedom system derived by Umeki & Kambe to analyse the experiments of Ciliberto & Gollub can be reduced to a two-

degree-of-freedom system because each non-axisymmetric mode has two completely degenerate components and the associated angular momentum of each mode tends to vanish owing to the damping and the circular symmetry.† Umeki (1989) discussed the relation between parameters in a Hamiltonian function and the symmetry of the shape of the container. Using Umeki & Kambe (1989) and the present study the controversy between the results of Meron & Procaccia (1989) and Miles (1989) concerning the existence of canonical formulations can be clarified.

Feng & Sethna (1989) have studied the bifurcations of surface waves in a slightly rectangular container both theoretically and experimentally. They gave explicit evaluations of nonlinear-term coefficients using the perturbation expansion method. Many of their experimental results were explained by their theoretical analysis. They predicted and observed travelling waves that are not addressed by SG (1989). Additionally Feng & Sethna (1989) predicted two different types of mixed wave states, although SG (1989) observed only one mixed wave in a square container and no mixed waves in a rectangular one. A direct comparison of Feng & Sethna (1989) and SG (1989) is difficult because dimensionless parameters σ and β in Feng & Sethna do not directly correspond to SG's (1989) experimental parameters, i.e. the amplitude and frequency of the external forcing. Nagata (1990) made a classification of stationary states of two completely degenerate modes (1, 0) and (0, 1) in a square container using nonlinear coefficients that varied with fluid depth. The general bifurcation problem of Faraday resonance in a square container was also studied by Silber & Knobloch (1989) using a two-dimensional map having D_4 symmetry. They suggested the necessity of fifth-order nonlinearity in their model in order to reproduce SG's (1989) diagram. An experiment similar to Ciliberto & Gollub (1985) was done by Karatsu (1988). He studied nearly degenerate (4, 1) and (1, 2) surface-wave modes in a circular cylinder, and observed periodic and chaotic mode competition. The experimental set-up and parameter-space diagram have been described in detail in Kambe & Umeki (1990), along with brief summary of Umeki & Kambe (1989) and the present study, which laid emphasis on comparison between experimental and theoretical results.

In the present paper, a general formula based on the average Lagrangian method, which is derived by Umeki & Kambe (1989), similar to Miles (1984*a*), including nonlinear capillary effects, is applied in order to study the mode interactions in a rectangular container. In §2, the nonlinear coefficients in some typical cases are evaluated. The previous results based on the perturbation method for the two-dimensional wave of Tadjbakhsh & Keller (1962), and for the three-dimensional wave of Verma & Keller (1962) and Feng & Sethna (1989), are confirmed using the presented Lagrangian approach, although the first two coefficients were previously given by Miles (1976).

In §3, an analysis of SG's (1989) experiments is made and the parameter-space diagrams are compared. A bifurcation diagram that includes Hopf bifurcation was obtained. Similar to the results of Feng & Sethna (1989), the presented stability diagram includes a mixed travelling wave state which was not observed by SG (1989). By numerically solving the third-order nonlinear model equations, periodic

† Crawford, Knobloch & Riecke (1990) pointed out that the additional phase instabilities, i.e. the rotation of wave patterns, may occur in a circular container; however, they misunderstood theoretical results of Umeki & Kambe (1989). Weakly nonlinear theory shows that the angular momentum of each mode tends to vanish, even if a mixed standing wave is excited, owing to the *circular* symmetry and linear damping. Notice that this property does not hold for a *rectangular* container, see below.

and non-periodic orbits in the phase space are shown. In §4, the unforced Hamiltonian system with specific coefficients is shown to have a homoclinic orbit, and also that if forcing is added, both the stable and unstable manifolds intersect transversally. Holmes (1986) proved homoclinic chaos for 2:1:2 external–internal resonance, and this was numerically found in the present study for 2:1:1 external–internal resonance. The Melnikov function was calculated using a reduction method, under the assumption that the forcing and damping are small perturbations to an unperturbed integrable system. In the Appendix, a method of determining whether the Hopf bifurcation of the Mb state is subcritical or supercritical is described using calculation of the centre manifold. The effect of fifth- and higher-order nonlinearity on this Hopf bifurcation is also discussed.

All results presented here are obtained by using the third-order nonlinear Hamiltonian system with linear damping. Higher-order nonlinearity, possibly achieved by changing the small parameters of slow timescale and nonlinearity, is not considered in the present study because the corresponding coefficients are not specified. The third-order model equation must be quantified before higher-order models are introduced. The efficiency of the third-order model equation is supported by the study of horizontally forced surface waves by Funakoshi & Inoue (1988) and also by Nobili *et al.* (1988), who demonstrated the coincidence between the experimental and numerical results.

2. Formulation of nonlinear dynamics of surface waves

Weakly nonlinear surface waves in a rectangular cylinder of an inviscid liquid with a density ρ are considered. Let (x, y) and z be the horizontal and vertical fixed reference coordinates of a container C having a cross-section S which is assumed to be independent of z, and with $\boldsymbol{n}$ being an outward vector normal to C. Let the boundary of S be denoted by ∂S, with the free surface and the bottom being respectively denoted by $z = \eta(t, x, y)$ and $z = -d$, where d is the depth of the undisturbed fluid. Assume that the flow is irrotational, thus allowing the velocity relative to C to be expressed by a velocity potential $\phi(t, x, y, z)$, i.e. $\boldsymbol{v} = \boldsymbol{\nabla}\phi$.

The solution can be expressed in expansion form as

$$\phi(t, x, y, z) = \sum_i \phi_i(t)\, \psi_i(x, y)\, \operatorname{sech} \kappa_i d \cosh \kappa_i (z + d), \tag{2.1a}$$

$$\eta(t, x, y) = \sum_i \eta_i(t)\, \psi_i(x, y), \tag{2.1b}$$

where $\{\psi_i\}$ is the eigenfunction of the linear system;

$$\left(\frac{\partial^2}{\partial x^2} + \frac{\partial^2}{\partial y^2} + \kappa_i^2\right)\psi_i = 0, \tag{2.2a}$$

with

$$\boldsymbol{n} \cdot \boldsymbol{\nabla}\psi_i = 0 \quad \text{on} \quad \partial S, \tag{2.2b}$$

and

$$\int_S \psi_i \psi_j \, \mathrm{d}x \, \mathrm{d}y = S\delta_{ij}, \tag{2.2c}$$

where δ_{ij} is the Kronecker delta.

For a rectangular cylindrical container of length l_x by l_y, the eigenfunction is

$$\psi_i(x, y) \equiv \psi_{mn}(x, y) = \{(2 - \delta_{m0})\,(2 - \delta_{n0})\}^{\frac{1}{2}} \cos \frac{\mathrm{m}\pi x}{l_x} \cos \frac{n\pi y}{l_y}, \tag{2.3}$$

with the wavenumber $$\kappa_{mn} = \left\{\left(\frac{m}{l_x}\right)^2 + \left(\frac{n}{l_y}\right)^2\right\}^{\frac{1}{2}}\pi. \tag{2.4}$$

A corresponding natural frequency is given by

$$\omega_{mn} = \{g\kappa_{mn}\tanh\kappa_{mn}d(1+\lambda^2\kappa_{mn}^2)\}^{\frac{1}{2}}, \tag{2.5}$$

where $\kappa = (\gamma/\rho g)^{\frac{1}{2}}$ is the capillary length.

The acceleration g_z due to the external forcing is assumed to be sinusoidal with the angular frequency 2ω and the amplitude a_0:

$$g_z = 4a_0\omega^2\cos 2\omega t. \tag{2.6}$$

The amplitude of the displacement of the ith mode is represented by

$$\eta_i(t) = \epsilon a_i[p_i(\tau)\cos\omega t + q_i(\tau)\sin\omega t + \epsilon\{A_i\cos 2\omega t + B_i\sin 2\omega t + C_i\}], \tag{2.7}$$

where $a_i - (\kappa_i\tanh\kappa_i d)^{-1}$ and we put $p_i = q_i = 0$ except for the subharmonic resonant modes $i = (m_i, n_i)$, $i = 1, \ldots, l$ (l being the number of resonant modes), $\epsilon(\ll 1)$ is an expansion parameter defined following (2.32), and $\tau = \epsilon^2\omega t$ is a dimensionless slow time variable expression the modulation of wave amplitudes. The amplitudes p_i and q_i are respectively called in-phase and out of phase.

The explicit form of the Lagrangian function in terms of η and $\dot{\eta}$ was derived by Miles (1984a) without nonlinear capillarity, and by Umeki & Kambe (1989) with it. Substituting (2.7) into the Lagrangian function, averaging it by t over the period $2\pi/\omega$, requiring A_i, B_i, C_i to be stationary with respect to τ, using the hypotheses that nonlinearity, forcing, and resonance are of the same small order and balance each other, neglecting the $O(\epsilon^6)$ terms, and dividing it by $a^3\epsilon^4\omega^2(a \equiv a_1 \approx a_i,\ i = 2, \ldots, l)$, a dimensionless Lagrangian function is obtained:

$$\frac{\langle L\rangle}{a^3\epsilon^4\omega^2} = \frac{1}{2}\sum_{i=1}^{l}(\dot{p}_i q_i - p_i\dot{q}_i) + H, \tag{2.8}$$

where differentiation is performed with respect to τ and where H is a Hamiltonian function with q_i and p_i being the conjugate variables of generalized coordinates and momenta:

$$\begin{aligned} H = {} & \tfrac{1}{2}\{\beta_i(p_i^2+q_i^2) + A_0(p_i^2-q_i^2)\} + D'_{jlmn}(L^3_{jl}L^3_{mn} + 2L^4_{jm}L^4_{ln}) \\ & + E'_{jlmn}(3L^3_{jl}L^3_{mn} - 2L^4_{jm}L^4_{ln}) + F_{jlmn}(L^1_{jl}L^1_{mn} + L^2_{jl}L^2_{mn}) \\ & + G_{jlmn}L^3_{jl}L^3_{mn} + H_{jlmn}(L^3_{jm}L^3_{ln} + L^4_{jl}L^4_{mn} + L^4_{jm}L^4_{nl}), \end{aligned} \tag{2.9}$$

with

$$\beta_i = \frac{1-\omega_i^2/\omega^2}{2\epsilon^2} \approx \frac{\omega-\omega_i}{\epsilon^2\omega_1}, \tag{2.10}$$

$$A_0 = a_0/a\epsilon^2, \tag{2.11}$$

$$D'_{jlmn} = -\tfrac{1}{16}a^2 D_{jlmn}, \quad E'_{jlmn} = \frac{\lambda^2 ag}{64\omega^2}E_{jlmn}, \tag{2.12a, b}$$

$$(F, G, H)_{jlmn} = (f, g, h)_i C_{ijl}C_{imn}, \tag{3.13a, b, c}$$

$$f_i = -\frac{a}{16a_i}\left(1-\frac{\omega_i^2}{4\omega^2}\right)^{-1}\{\tfrac{3}{4} - \tfrac{1}{2}a\,a_i\kappa_i^2 + \tfrac{1}{8}a^2(2\kappa^2-\kappa_i^2)\}^2, \tag{2.14a}$$

$$g_i = \frac{a\omega^2}{32a_i\omega_i^2}\{1-\tfrac{1}{2}a^2(2\kappa^2-\kappa_i^2)\}^2, \quad h_i = \tfrac{1}{64}a^3 a_i\kappa_i^4, \tag{2.14b, c}$$

$$\kappa \equiv \kappa_1 \approx \kappa_i, \quad i = 2, \ldots, l, \tag{2.15}$$

$$C_{lmn} = S^{-1} \int_S \psi_l \psi_m \psi_n \, \mathrm{d}x \, \mathrm{d}y, \tag{2.16}$$

$$D_{jlmn} = S^{-1} \int_S \psi_j \psi_l \nabla\psi_m \cdot \nabla\psi_n \, \mathrm{d}x \, \mathrm{d}y, \tag{2.17a}$$

$$E_{jlmn} = S^{-1} \int^S (\nabla\psi_j \cdot \nabla\psi_l)(\nabla\psi_m \cdot \nabla\psi_n) \, \mathrm{d}x \, \mathrm{d}y, \tag{2.17b}$$

and

$$L^1_{ij} = p_i p_j - q_i q_j, \quad L^2_{ij} = p_i q_j + q_i p_j, \tag{2.18a, b}$$

$$L^3_{ij} = p_i p_j + q_i q_j, \quad L^4_{ij} = p_i q_j - q_i p_j \tag{2.18c, d}$$

Here the summation convention for the repeated indices (i, j, l, m, n) is used, except in (2.14)–(2.18). Several algebraic inconsistencies contained in Umeki & Kambe (1989) have been made corrected. (See (2.9), (2.10) and (2.14*a*, *b*).)

The presented formulae ((2.9)–(2.18)) are applied to analyse four special but typical gravity waves ($\lambda = 0$). They are: Case (*a*) a single three-dimensional mode (m, m) in a rectangular container having arbitrary lengths; Case (*b*) two degenerate two-dimensional modes $(m, 0)$, $(0, m)$; Case (*c*), two degenerate three-dimensional modes (m, n), (n, m) in a square container; and Case (*d*) a two-dimensional mode $(1, 0)$ and a three-dimensional mode $(1, 1)$ in a narrow rectangular container ($l_x \gg l_y$). In these cases the Hamiltonian function (2.9) is reduced to

$$H = \sum_i \{\tfrac{1}{2}\beta_i(p_i^2 + q_i^2) + \tfrac{1}{2}A_0(p_i^2 - q_i^2) + c_i(p_i^2 + q_i^2)^2\} + c_3(p_1^2 + q_1^2)(p_2^2 + q_2^2) + c_4(p_1 q_2 - q_1 p_2)^2, \tag{2.19}$$

where the c_2, c_3, and c_4 terms vanish only for Case (*a*), and the coefficients c_i are given by

$$c_1 = D'_1 + 3E'_1 + F_1 + G_1 + H_1, \tag{2.20a}$$

$$c_2 = D'_2 + 3E'_2 + F_2 + G_2 + H_2, \tag{2.20b}$$

$$c_3 = D'_3 + D'_4 + 4D'_5 + 6E'_3 + 12E'_5 + 2F_3 + 4F_5 + 2G_3 + 4G_5 + 2H_3 + 4H_5, \tag{2.20c}$$

$$c_4 = 2D'_3 + 2D'_4 - 8D'_5 - 4E'_3 - 8E'_5 - 4F_3 - 4G_5 - 4H_3, \tag{2.20d}$$

with the subscripts being denoted as $\mathbf{1} = (1, 1, 1, 1)$, $\mathbf{2} = (2, 2, 2, 2)$, $\mathbf{3} = (1, 1, 2, 2)$, $\mathbf{4} = (2, 2, 1, 1)$, $\mathbf{5} = (1, 2, 1, 2)$, and ordered as (j, l, m, n). Here the relations $E'_3 = E'_4$, $F_3 = F_4$, $G_3 = G_4$, and $H_3 = H_4$ hold. The summation in (2.19) is used for $i = 1$ for Case (*a*) and $i = 1, 2$ for Cases (*b*)–(*d*).

Case (*a*): *single three-dimensional mode*

Harmonic resonant modes which interact with a mode $1 = (m, m)$ are $2 = (2m, 0)$, $3 = (0, 2m)$, and $4 = (2m, 2m)$. Non-vanishing correlation integrals (2.16), (2.17*a*) are

$$C_{112} = C_{113} = 1/\sqrt{2}, \quad C_{114} = \tfrac{1}{2}, \tag{2.21a, b}$$

$$D_{1111} = \tfrac{3}{4}\kappa^2. \tag{2.21c}$$

The coefficient c_1, (2.20*a*), is given by

$$c_1 = \frac{1}{128}\left[-\frac{4T\{3 + T^{-2}(1 - \tilde{\kappa}_2^2)\}^2}{4T - \tilde{\kappa}_2 T_2} - \frac{4T\{3 + T^{-2}(1 - \tilde{\kappa}_3^2)\}^2}{4T - \tilde{\kappa}_3 T_3} \right.$$
$$\left. + 23 - \tfrac{5}{2}T^{-2} + \tfrac{3}{4}(\tilde{\kappa}_2^4 + \kappa_3^4)\, T^{-4} - \tfrac{9}{2}T^{-6} \right], \tag{2.22}$$

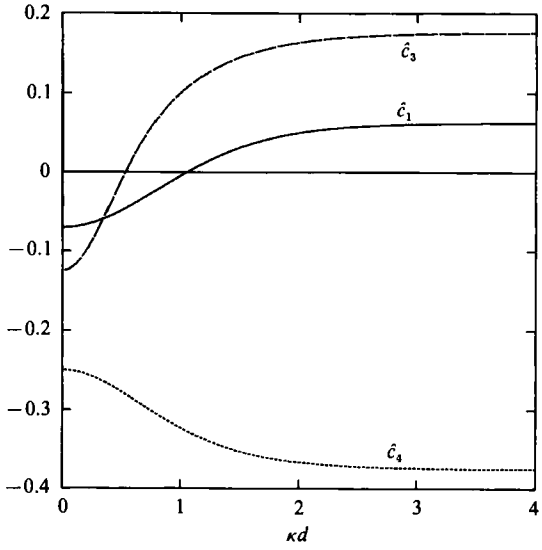

FIGURE 1. Normalized nonlinear coefficients $\hat{c}_1$, $\hat{c}_3$, $\hat{c}_4$ for two degenerate two-dimensional modes of gravity waves in a square container versus dimensionless fluid depth κd. See (2.24*a–c*).

where $T = \tanh \kappa d$, $T_i = \tanh \kappa_i d$ and $\tilde{\kappa}_i = \kappa_i/\kappa$ $(i = 2, 3)$. The relation

$$f_i + g_i + h_i = \frac{1}{64}\left[-\frac{4T\{3+T^{-2}(1-\tilde{\kappa}_i^2)\}^2}{4T-\tilde{\kappa}_i T_i} + 11 + (2-\tilde{\kappa}_i^2)\,T^{-2} + \tfrac{3}{4}(2-\tilde{\kappa}_i^2)^2 T^{-4}\right]$$

was used to calculate (2.22). Expression (2.22) agrees with Verma & Keller (1962) and Miles (1976).

Case (b): two degenerate two-dimensional modes in a square container

Harmonic modes interacting with $1 = (m, 0)$, $2 = (0, m)$, and both 1, 2 are respectively $3 = (2m, 0)$, $4 = (0, 2m)$, and $5 = (m, m)$. Correlation integrals are given by

$$C_{113} = C_{224} = 1/\sqrt{2}, \quad C_{125} = 1, \tag{2.23a, b}$$

$$D_{1111} = D_{2222} = \tfrac{1}{2}\kappa^2, \quad D_{1122} = D_{2211} = \kappa^2, \quad D_{1212} = 0. \tag{2.23c, d, e}$$

The coefficients c_i defined by (2.20*a–d*) are

$$c_1 = c_2 = \tfrac{1}{128}(2 + 3T^{-2} + 12T^{-4} - 9T^{-6}), \tag{2.24a}$$

$$c_3 = \frac{1}{16}\left\{-\frac{4T(3-T^{-2})^2}{4T-\sqrt{2}T_5} + 11 - 2T^{-2}\right\}, \tag{2.24b}$$

$$c_4 = -\tfrac{1}{8} - \tfrac{1}{4}T^{-2}. \tag{2.24c}$$

The expressions (2.24*a–c*) agree with Tadjbakhsh & Keller's (1960) results (see Miles 1976) and (2.15) of Feng & Sethna (1989) where the equality below holds:

$$\frac{1}{\omega_{mn}^4}(\pi_1, \pi_2, \pi_3) = \tfrac{1}{2}(-4c_1, -2c_3 - c_4, c_4). \tag{2.25}$$

Figure 1 shows the coefficients $(\hat{c}_1, \hat{c}_3, \hat{c}_4) = (c_1 T^6, c_3 T^4, c_4 T^2)$ versus the dimensionless fluid depth, κd. This normalization was chosen to avoid the divergence in the shallow water limit as $\kappa d \to 0$. It should be noted that the ratios of the mode-coupling constants c_3 and c_4 to the single-mode nonlinear coefficient c_1 approach zero as the dimensionless depth approaches zero. However, the normalized $\hat{c}_i$ values coincide with original c_i values in the deep-water limit as $\kappa d \to \infty$.

Case (c): two degenerate three-dimensional modes in a square container

The resonant modes are correspondingly numbered as $1 = (m, n)$, $2 = (n, m)$, $3 = (2m, 0)$, $4 = (0, 2n)$, $5 = (2m, 2n)$, $6 = (2n, 0)$, $7 = (0, 2m)$, $8 = (2n, 2m)$, $9 = (|m-n|, |m-n|)$, $\widehat{10} = (|m-n|, m+n)$, $\widehat{11} = (m+n, |m-n|)$, $\widehat{12} = (m+n, m+2)\,(m \neq n)$. A circumflex is used to distinguish mode numbers from double modes (i.e. 11 from 1 and 1, etc). Non-vanishing correlation integrals are given as

$$C_{113} = C_{114} = C_{226} = C_{227} = 1/\sqrt{2}, \tag{2.26a}$$

$$C_{115} = C_{228} = C_{129} = C_{12\widehat{10}} = C_{12\widehat{11}} = C_{12\widehat{12}} = \tfrac{1}{2}, \tag{2.26b}$$

$$D_{1111} = D_{2222} = \tfrac{3}{4}\kappa^2, \quad D_{1122} = D_{2211} = \kappa^2, \quad D_{1212} = 0. \tag{2.26c,d,e}$$

The equalities of the factors f_i, g_i, h_i for $i = 3$ and 7, 4 and 6, 5 and 8, and 10 and 11 hold owing to the symmetry of the system resulting from a 90° rotation transformation. The coefficients are given by

$$c_1 = c_2 = \frac{1}{128}\Bigg[-\frac{4T\{3+T^{-2}(1-\tilde{\kappa}_3^2)\}^2}{4T-\tilde{\kappa}_3 T_3} - \frac{4T\{3+T^{-2}(1-\tilde{\kappa}_4^2)\}^2}{4T-\tilde{\kappa}_4 T_4} + 23 - \tfrac{5}{2}T^{-2} + \tfrac{3}{4}(\tilde{\kappa}_3^4+\tilde{\kappa}_4^4)\,T^{-4} - \tfrac{9}{2}T^{-6}\Bigg], \tag{2.27a}$$

$$c_3 = \frac{1}{64}\Bigg[-\frac{4T\{3+T^{-2}(1-\tilde{\kappa}_9^2)\}^2}{4T-\tilde{\kappa}_9 T_9} - \frac{4T\{3+T^{-2}(1-\tilde{\kappa}_{12}^2)\}^2}{4T-\tilde{\kappa}_{12} T_{12}} - \frac{8T(3-T^{-2})^2}{4T-\sqrt{2}T_{10}} + 44 - 8T^{-2} + \tfrac{3}{4}(-8+\tilde{\kappa}_9^4+\tilde{\kappa}_{12}^4)\,T^{-4}\Bigg], \tag{2.27b}$$

$$c_4 = -\tfrac{1}{32}\{4+8T^{-2}+\tfrac{1}{4}(-8+\tilde{\kappa}_9^4+\tilde{\kappa}_{12}^4)\,T^{-4}\}, \tag{2.27c}$$

The equality (2.25) is in agreement with Feng & Sethna (1989) if the factor $\frac{1}{2}$ on the right-hand side is instead unity. Expression (2.14*c*) of Feng & Sethna is misprinted, i.e. a 1 should be added in the square bracket. In the two-dimensional limit, $m/n \to \infty$, the coefficient c_1, (2.27*a*), differs from that of the two-dimensional case (2.24*a*), as is pointed out by Verma & Keller (1962), yet the mode-coupling constants c_3 and c_4 coincide with the two-dimensional values (2.24*b*, *c*). Figure 2 shows the nonlinear coefficients normalized as $(\hat{c}_1, \hat{c}_3, \hat{c}_4) = (c_1 T^6,\ c_3 T^6,\ c_4 T^4)$, as a function of the dimensionless fluid depth κd for the two-dimensional limit and $(\hat{c}_1, \hat{c}_3, \hat{c}_4) = (c_1 T^6, c_3 T^4, c_4 T^2)$ for $m/n = 1$.

Case (d): two modes (1, 0), (1, 1) *in a narrow rectangular container*

Modes are numbered as $1 = (1, 0)$, $2 = (1, 1)$, $3 = (2, 0)$, $4 = (0, 2)$, $5 = (2, 2)$, $6 = (0, 1)$, $7 = (2, 1)$. Assume $l_x \ll l_y$ and $\pi d/l_y \ll 1$, and neglect the $O((l_x/l_y)^2, (\pi d/l_y)^2)$ terms. Non-vanishing correlation integrals are given by

$$D_{1111} = D_{1122} = D_{2211} = D_{1212} = \tfrac{1}{2}\kappa^2, \quad D_{2222} = \tfrac{3}{4}\kappa^2, \tag{2.28a, b}$$

$$C_{113} = C_{223} = C_{224} = C_{127} = 1/\sqrt{2}, \quad C_{126} = 1, \quad C_{225} = \tfrac{1}{2}. \tag{2.28c, d, e}$$

The coefficients c_1, c_2, c_3, c_4 defined by (2.20*a–d*) are given by

$$c_1 = \tfrac{1}{128}(2+3T^{-2}+12T^{-4}-9T^{-6}), \quad c_2 = \tfrac{1}{256}(10+T^{-2}+40T^{-4}-27T^{-6}), \tag{2.29a, b}$$

$$c_3 = \tfrac{1}{64}(14-7T^{-2}+44T^{-4}-27T^{-6}), \quad c_4 = \tfrac{1}{32}(-6-2T^{-2}-8T^{-4}+9T^{-6}). \tag{2.29c, d}$$

Figure 3 shows the coefficients $\hat{c}_i = c_i T^6$ for $i = 1, \ldots, 4$.

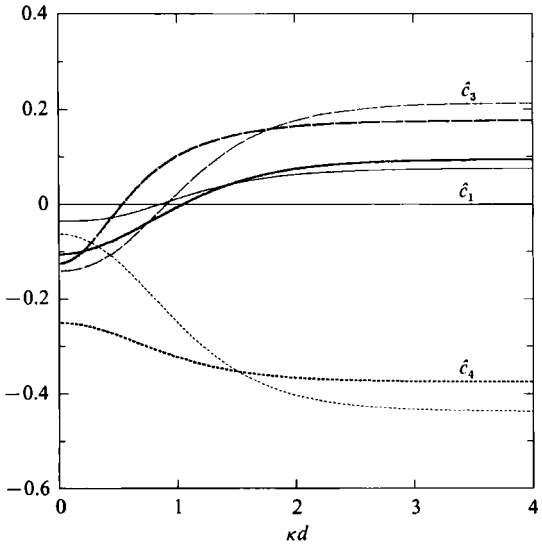

FIGURE 2. Normalized nonlinear coefficients $\hat{c}_1$, $\hat{c}_3$, $\hat{c}_4$ for two degenerate three-dimensional modes of gravity waves in a square container versus dimensionless fluid depth κd. Thick and thin curves denote the two-dimensional limit $m/n \to \infty$ and $m/n = 1$, respectively. See (2.27*a–c*).

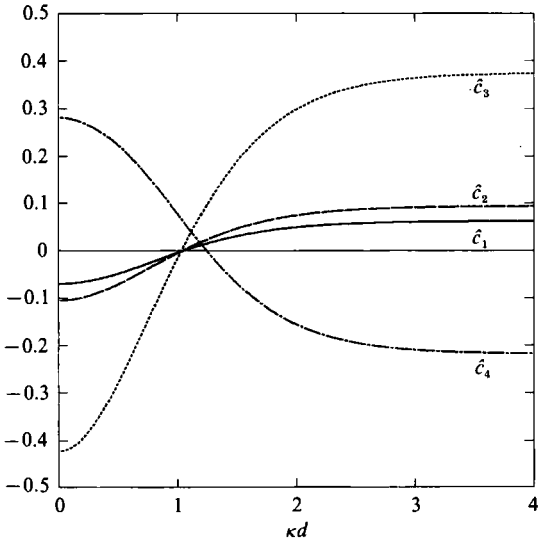

FIGURE 3. Normalized nonlinear coefficients $\hat{c}_1$, $\hat{c}_2$, $\hat{c}_3$, $\hat{c}_4$ for a two-dimensional mode (1, 0) and a three-dimensional mode (1, 1), being nearly degenerate in a narrow rectangular container, versus non-dimensional fluid depth κd. The coefficients are multiplied by the factor T^6 for normalization. See (2.29*a–d*).

Results corresponding to SG's (1989) experiment, i.e. two modes: $1 = (m, n) = (3, 2)$ and $2 = (n, m) = (2, 3)$, are now presented. The coefficients c_i, including nonlinear capillary effects, are given by (2.20*a–d*) with (2.12*a*)–(2.17*b*), where the summation is similar to Case (*c*). Two modifications caused by the surface tension must be incorporated. One is the term E'_{jlmn} in (2.20) and the other is the shift of the natural

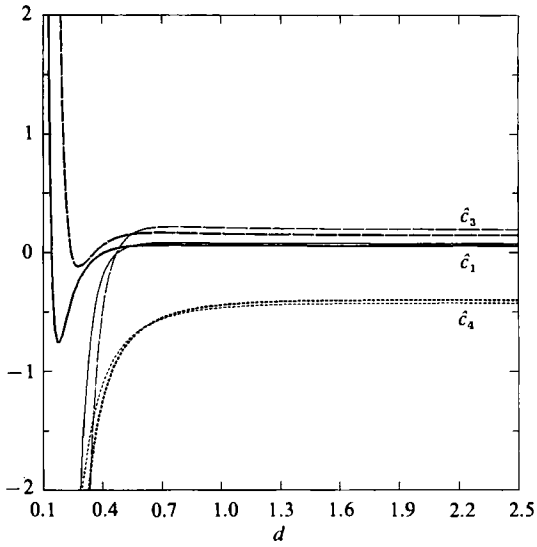

FIGURE 4. Normalized nonlinear coefficients c_i versus d for two three-dimensional modes (3, 2) and (2, 3), corresponding to the experiment of SG (1989). Thin (thick) curve denotes the value without (with) the surface tension. See (2.20).

frequencies ω_i. The term E'_{jlmn} in (2.20) is negligible, only a few percent of the other terms, although the shift of ω_i is not negligible in F_i when the fluid is shallow ($\kappa d \ll 1$).

The parameters used by SG (1989) were $d = 2.5$ cm, $l_x = l_y = 6.17$ cm for the square case and $(l_x, l_y) = (6.17,\ 6.6)$ cm for the slightly rectangular case. The wavelength was $\kappa^{-1} \approx a \approx 5.8$ mm. An n-butyl alcohol solution was chosen as the container liquid, having capillary length $\lambda = 0.176$ cm. Figure 4 shows the dependence of c_i on the depth d for the square container with a fixed $\omega = \frac{1}{2}(\omega_1 + \omega_2)$. There are no 1:2 internal resonances for the gravity wave (thin curve) that cause the c_i coefficients to diverge. The dependence of c_i on the external frequency ω was also examined, but c_i changed by less than a few percent and their signs remained the same when the value of $f_0 (\equiv \omega/\pi)$ was between 13.45 and 13.90 Hz. The experimentally observed natural frequencies were often slightly different from the values obtained using (2.5), even when capillarity is taken into account. Thus the natural frequencies in β_i can be replaced by $\omega_i = \pi f_i$, with $f_1 = 13.60$ Hz and $f_2 = 13.80$ Hz for the rectangular case, and $f_1 = f_2 = 14.10$ for the square case. The minimum excitation external-forcing amplitude $2a_{0\min}$ for excitation was taken at 120 and 140 μm. Values of calculated nonlinear coefficients were

$$(\hat{c}_1, \hat{c}_3, \hat{c}_4) = (0.0756,\ 0.193,\ -0.428) \tag{2.30}$$

without capillarity and

$$(\hat{c}_1, \hat{c}_3, \hat{c}_4) = (0.0569, 0.144,\ -0.44) \tag{2.31}$$

with it.

Using the Hamiltonian function (2.19), two-degree-of-freedom nonlinear evolution equations of two subharmonic modes are given by

$$\frac{\mathrm{d}}{\mathrm{d}\tau}(p_i, q_i) = \left(-\frac{\partial}{\partial q_i}, \frac{\partial}{\partial p_i}\right) H - \alpha(p_i, q_i), \quad i = 1, 2. \tag{2.32}$$

Here, linear damping terms are phenomenologically introduced on the right-hand side, so as to express the dissipation effect in real fluids, which is important for the surface waves in a container. A small expansion parameter, ϵ, is chosen as $[(\omega_2^2-\omega_1^2)/2\omega^2]^{\frac{1}{2}}$ and ≈ 0.12, so that the relation $\beta_1-\beta_2=1$ will hold for the rectangular case. A corresponding damping coefficient is $\alpha = a_{0\min}/a\epsilon^2$. For the square, ϵ is taken as $(a_{0\min}/a)^{\frac{1}{2}}$ so that the damping coefficient α is unity. In this and the next section, the parameter β_i, α, and A_0 are assumed to be within the same order, and thus the results are not dependent on the selection of ϵ. As long as β_i, α, A_0, p_i, and q_i are bounded within the order 1, and ϵ remains small, the higher nonlinear terms neglected in the presented analysis are evaluated as $O(\epsilon^2)$ and do not affect the stability given by the third-order nonlinear model equations.

The angular momentum associated with rotation of the wave patterns is defined by

$$L_{\text{a.m.}} = \rho \int_0^{l_x}\int_0^{l_y}\int_{-d}^{\eta}\left(x\frac{\partial\phi}{\partial y}-y\frac{\partial\phi}{\partial x}\right)\mathrm{d}x\,\mathrm{d}y\,\mathrm{d}z. \tag{2.33}$$

Using (2.1), (2.3) and $\phi_t = a_i\dot{\eta}_i+O(\epsilon^2)$, the angular momentum up to $O(\epsilon^2)$ in a square container can be expressed as

$$L_{\text{a.m.}} = \rho a^3\epsilon^2\omega\frac{16(m^2+n^2)l_x^2}{(m^2-n^2)^3\pi^2}(p_1q_2-p_2q_1), \tag{2.34}$$

for modes $1=(m,n)$ and $2=(n,m)$ with an odd integer $m+n$, and

$$L_{\text{a.m.}} = \rho a^3\epsilon^2\omega\frac{8l_x^2}{m^2\pi^2}(p_1q_w-p_2q_1), \tag{2.35}$$

for modes $1=(m,0)$ and $2=(0,m)$ with an odd m. When $m+n$ or m is even, the integral in (2.33) vanishes and the total angular momentum is zero.

3. Analysis of the dissipative dynamical equations

The evolution equations for slowly varying amplitudes (p_i, q_i) of two nearly or completely degenerate subharmonic modes are expressed as a system of equations,

$$\dot{p}_1 = -\alpha p_1+(-\beta_1+A_0-A_1r_1^2-Cr_2^2)q_1+DMp_2, \tag{3.1a}$$

$$\dot{q}_1 = -\alpha q_1+(\beta_1+A_0+A_1r_1^2+Cr_2^2)p_1+DMq_2, \tag{3.1b}$$

$$\dot{p}_2 = -\alpha p_2+(-\beta_2+A_0-A_2r_2^2-Cr_1^2)q_2-DMp_1, \tag{3.1c}$$

$$\dot{q}_2 = -\alpha q_2+(\beta_2+A_0+A_2r_2^2+Cr_1^2)p_2-DMq_1, \tag{3.1d}$$

where $M=p_1q_2-p_2q_1$, $r_i^2=p_i^2+q_i^2$, $A_i=4c_i$ for $i=1,2$, $C=2c_3$ and $D=2c_4$. A_1 and A_2 are distinguished from each other so that this analysis can be applied to a more general case ($c_1\neq c_2$) like two internally resonant modes in a circular cylindrical container in addition to the presented system having square symmetry. Eight independent parameters, $A_1, A_2, C, D, \alpha, \beta_1, \beta_2, A_0$, can be reduced to six by rescaling p_i, q_i, and τ.

There are four types of stationary states of the system (3.1 *a–d*). They are annotated as a quiescent state (Q), a single mode-i standing wave (Si) and mixed standing wave (M). Note that mixed standing wave states are later classified as rotating and non-rotating waves. The quiescent state is linearly unstable if $A_0 > (\beta_i^2-\alpha^2)^{\frac{1}{2}}$ for $i=1$ or 2.

The stability of the Si state is obtained by solving eigenvalues of the linear equation with respect to a small perturbation $(\tilde{p}_1, \tilde{q}_1, \tilde{p}_2, \tilde{q}_2)\,e^{\lambda\tau}$. Calculations yield two quadratic equations:

$$\lambda^2+2\alpha\lambda+4[A_0^2-\alpha^2\mp\beta_m(A_0^2-\alpha^2)^{\frac{1}{2}}]=0, \tag{3.2a}$$

$$\lambda^2+2\alpha\lambda+A_m^{-2}\{(C-A_m)(A_0^2-\alpha^2)^{\frac{1}{2}}\pm(A_m\beta_n-C\beta_m)\}\times[(A_m+C+D)(A_0^2-\alpha^2)^{\frac{1}{2}}\pm\{A_m\beta_n-(C+D)\beta_m\}]=0, \tag{3.2b}$$

where $(m,n)=(1,2)$ for $i=1$ and $(2,1)$ for $i=2$. Note that the first and second equations respectively indicate the stability in the direction of mode-m and -n. Si_- is always unstable in the direction of mode-i; however, Si_+ is unstable in the direction of mode-j $[(i,j)=(1,2)$ and $(2,1)]$ if the constant term in (3.2b) is negative.

The fixed points of all non-zero components can be solved as follows. Rearranging the (3.1a–d) system into the form

$$A_m\begin{pmatrix}p_m\\q_m\end{pmatrix}=0, \tag{3.3a}$$

where $$A_m=\begin{pmatrix}-\alpha+Dp_nq_n & -\beta_m+A_0-A_mr_m^2-Cr_n^2-Dp_n^2\\ \beta_m+A_0+A_mr_m^2+Cr_n^2+Dq_n^2 & -\alpha-Dp_nq_n\end{pmatrix}, \tag{3.3b}$$

$(m,n)=(1,2)$ corresponds to (3.1a,b), and $(m,n)=(2,1)$ to (3.1c,d). Setting the determinant of (3.3b) to zero leads to

$$\alpha^2-A_0^2+(\beta_m+A_mr_m^2+Cr_n^2)\{\beta_m+A_mr_m^2+(C+D)r_n^2\}+A_0D(p_n^2-q_n^2)=0. \tag{3.4}$$

Multiplying the upper rows of (3.3a) by q_m, the lower rows by p_m, and taking the difference between them gives

$$A_0(p_m^2-q_m^2)=-(\beta_m+A_mr_m^2+Cr_n^2)r_m^2-DM^2. \tag{3.5}$$

Substituting (3.5) into (3.4) yields

$$\alpha^2-A_0^2+(\beta_m+A_mr_m^2+Cr_n^2)\{\beta_m+A_mr_m^2+(C+D)r_n^2\}-D(\beta_n+A_nr_n^2+Cr_m^2)r_n^2-D^2M^2=0. \tag{3.6}$$

Taking the difference between (3.6) for $(m,n)=(1,2)$ and for $(m,n)=(2,1)$ respectively leads to

$$\Delta\beta+(A_1-C)r_1^2+(C-A_2)r_2^2=0, \tag{3.7}$$

or

$$\beta_1+\beta_2+(A_1+C+D)r_1^2+(A_2+C+D)r_2^2=0, \tag{3.8}$$

where $\Delta\beta=\beta_1-\beta_2(\equiv 1$ for the slightly rectangular container, and 0 for the square). The mixed modes that satisfy (3.7) and (3.8) are respectively denoted Ma and Mb.

If the system (3.1a–d) is placed in a matrix form with $\mathrm{d}/\mathrm{d}r=0$, then

$$\boldsymbol{M}\begin{pmatrix}p_1\\q_1\\p_2\\q_2\end{pmatrix}=0.$$

If the determinant of $\boldsymbol{M}$ is required to vanish, an expression for M is as

$$D^2M^2=(\beta_1+A_1r_1^2+Cr_2^2)(\beta_2+A_2r_2^2+Cr_1^2)-A_0-\alpha^2\pm\mathrm{Det}^{\frac{1}{2}}, \tag{3.9}$$

where

$$\mathrm{Det}=A_0^2\{\Delta\beta+(A_1-C)r_1^2+(C-A_2)r_2^2\}^2-\alpha^2\{\beta_1+\beta_2+(A_1+C)r_1^2+(A_2+C)r_2^2\}^2+4A_0^2\alpha^2. \tag{3.10}$$

Substituting (3.9) into (3.6) with $(m,n)=(1,2)$ and $(2,1)$, and adding them leads to

$$\mathrm{Det}=(2\alpha^2+\tfrac{1}{2}UV)^2, \tag{3.11}$$

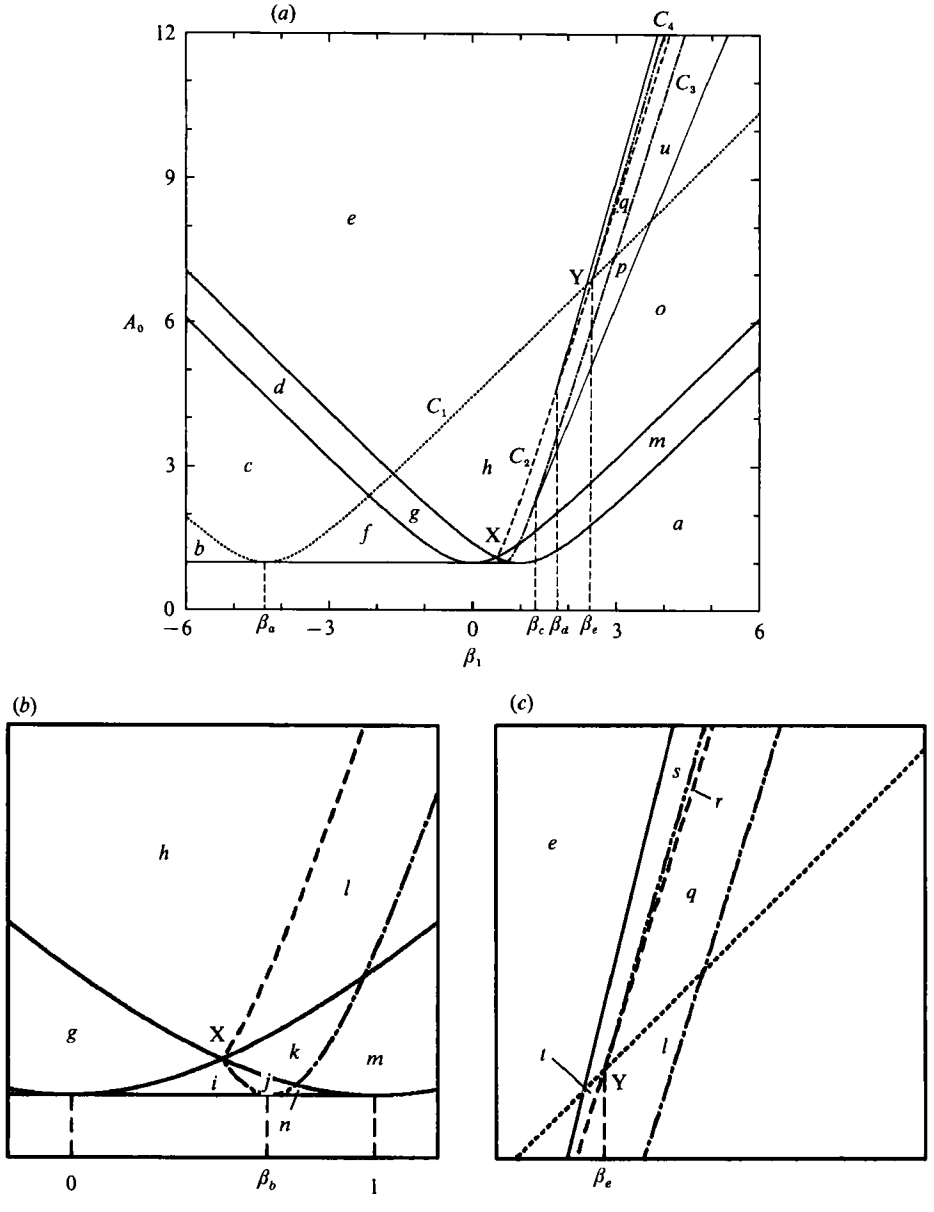

FIGURE 5. (*a*) Parameter-space diagram in the (A_0, β_1) plane for the rectangular case. Bifurcation curves of Ma from S1, of Mb from S1 and from S2, and a curve of exchange of stability between Ma and Mb are denoted respectively by C_1, C_2, C_3 and C_4. (*b*) An enlargement of the region near point X and (*c*) near point Y. Stationary states in each region and their stabilities are classified in table 1.

where
$$U = \Delta\beta + (A_1 - C)\, r_1^2 + (C - A_2)\, r_2^2, \tag{3.12a}$$
$$V = \Delta\beta + (A_1 - C - D)\, r_1^2 + (C + D - A_2)\, r_2^2. \tag{3.12b}$$

For the Ma state, equating (3.10) and (3.11) yields
$$\beta_1 + A_1 r_1^2 + C r_2^2 = \pm (A_0 - \alpha^2)^{\frac{1}{2}}. \tag{3.13}$$

	Q	$S1_+$	$S1_-$	$S2_+$	$S2_-$	Ma_+	Ma_-	Mb
a	S	/	/	/	/	/	/	/
b	S	U	U	U	U	S	U	/
c	S	U	U	U	U	S	/	/
d	U	U	/	U	U	S	/	/
e	U	U	/	U	/	S	/	/
f	S	S	U	U	U	/	/	/
g	U	S	/	U	U	/	/	/
h	U	S	/	U	/	/	/	/
i	S	/	/	S	U	/	/	/
j	S	/	/	U	U	/	/	(U, S)
k	U	/	/	U	U	/	/	(U, S)
l	U	U	/	U	/	/	/	S
m	U	/	/	S	/	/	/	/
n	S	/	/	S	/	/	/	/
o	U	U	/	S	/	/	/	/
p	U	/	/	S	/	/	/	[S, U]
q	U	S	/	U	/	U	/	S
r	U	S	/	U	/	U	/	[S, U]
s	U	U	/	U	/	S	/	[S, U]
t	U	S	/	U	/	/	/	[S, U]
u	U	S	/	S	/	U	/	[S, U]

TABLE 1. Classification of fixed points. S, U and / denote stable, unstable and no fixed points, respectively. (U, S) denotes U or S and [S, U] the multiplicity of stable and unstable Mb states.

Substituting (3.13) into (3.9) and using (3.7) leads to

$$M = 0. \tag{3.14}$$

This indicates that the Ma state is non-rotating.

The Mb state can be obtained in an implicit form. Equating (3.10) and (3.11) and using (3.8) yields

$$A_0 = \left[\frac{(2\alpha^2 + \tfrac{1}{2}UV)^2 + \alpha^2 D^2 (r_1^2 + r_2^2)^2}{U^2 + 4\alpha^2}\right]^{\frac{1}{2}}. \tag{3.15}$$

Using the values (2.30), the nonlinear-term coefficients for both a square and a slightly rectangular container are given by

$$A_1 = A_2 = 0.26, \quad C = 0.32, \quad D = -0.80. \tag{3.16a, b, c}$$

Note that these values satisfy the inequalities

$$C > A > 0, \quad D < 0, \quad A + C + D < 0, \tag{3.17}$$

which are equivalent to (2.17) of Feng & Sethna (1989). The case $A_1 \neq A_2$ was examined for the slightly rectangular container, but the difference between A_1 and A_2 was small and did not significantly affect the following presented results. The difference is considered as higher-order effects and is important if nonlinear effects higher than third-order are included. However, $\Delta\beta$ is an important factor in the presented analysis.

3.1. *Slightly rectangular case*

Using (3.7), (3.13) and (3.16), two Ma states can be distinguished: a larger amplitude one Ma_+ and a smaller amplitude one Ma_-, and they exist in the regions as

$$Ma_\pm: \quad \beta_1 < \frac{A_1}{A_1 - C} \pm (A_0^2 - \alpha^2)^{\frac{1}{2}}. \tag{3.18}$$

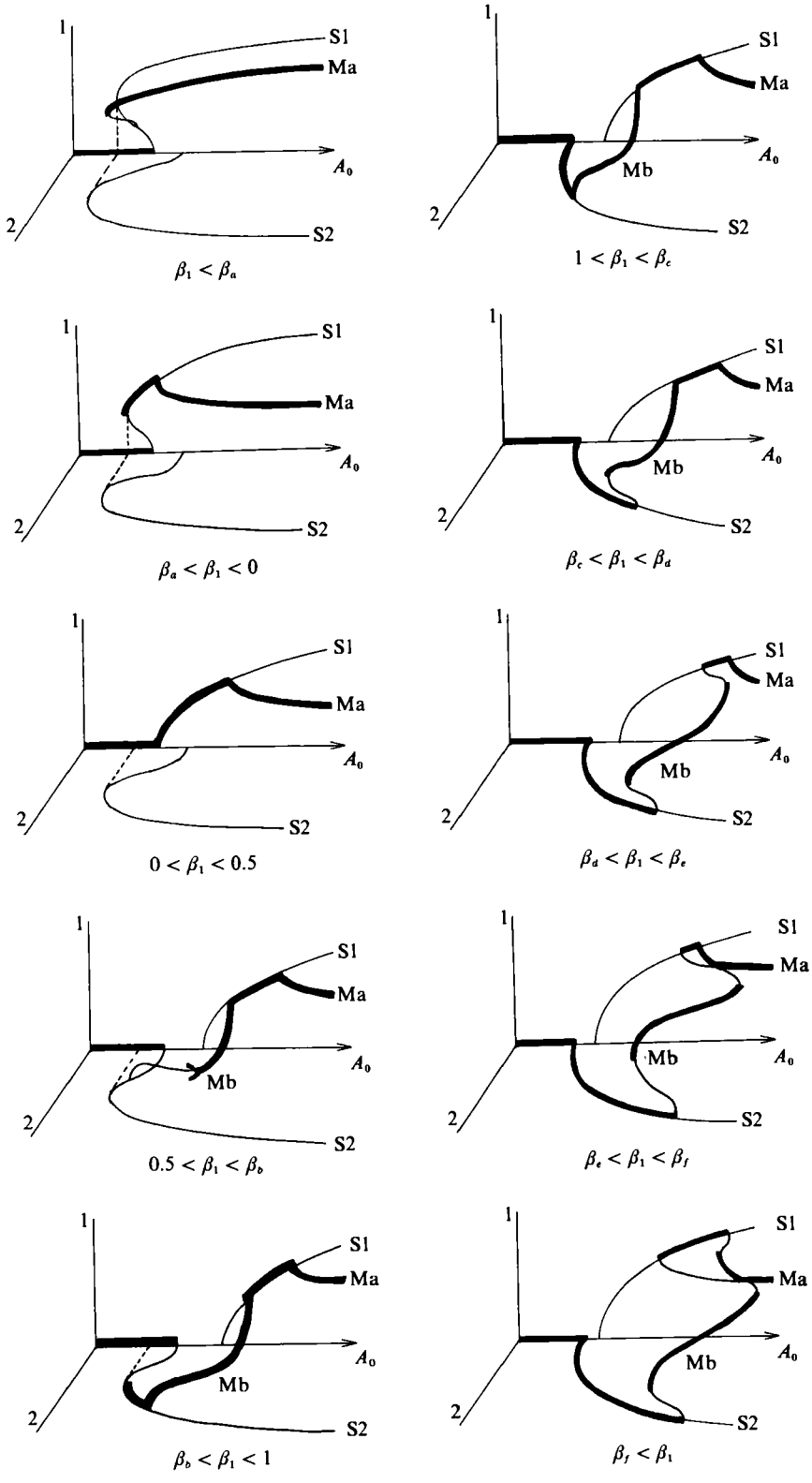

FIGURE 6. For caption see facing page.

The Ma-state bifurcation curves from S1 are given by

$$C_1: \quad A_0 = \left\{\alpha^2 + \left(\frac{A_1\beta_2 - C\beta_1}{A_1 - C}\right)^2\right\}^{\frac{1}{2}}. \tag{3.19}$$

The Mb state satisfies the relation

$$\beta_1 + \beta_2 + (A_1 + C + D)(r_1^2 + r_2^2) = 0, \tag{3.20}$$

and must satisfy $\beta_1 + \beta_2 > 0$ because $A_1 + C + D < 0$. The bifurcation curves from S1 and S2 are given by

$$C_2: \quad A_0 = \left\{\alpha^2 + \left(\frac{-A_1\beta_2 + (C+D)\beta_1}{A_1 + C + D}\right)^2\right\}^{\frac{1}{2}}, \tag{3.21a}$$

and

$$C_3: \quad A_0 = \left\{\alpha^2 + \left(\frac{-A_1\beta_1 + (C+D)\beta_2}{A_1 + C + D}\right)^2\right\}^{\frac{1}{2}}. \tag{3.21b}$$

A numerical calculation in the experimentally investigated range of the forcing frequency and amplitude near the intersection point X (codimension-2 bifurcation point) of two instability curves of a quiescent state shows that A_0, solved by (3.15) between $r_1^2 = 0$ and $-(\beta_1 + \beta_2)/(A_1 + C + D)$, is increasing monotonically, thus there exists a single Mb state between two bifurcation curves (3.21*a*) and (3.21*b*). However, as f_0 increases a multiplicity of Mb states is found. The stabilities of the Mb and Ma states were examined by a numerical calculation of eigenvalues of the linear equation of a small perturbation. It is found that Mb state becomes unstable (i.e. a Hopf bifurcation occurs) on the right-hand side of the point X. This type of Hopf bifurcation of mixed modes is interpreted as follows. The Mb state bifurcated from S1 is stable because S1 is stable as a result of its supercritical origin, yet the Mb state bifurcated from S2, which arises via a subcritical bifurcation, is unstable and loses its stability between the curves C_2 and C_3. A similar bifurcation with respect to the mode competition was shown by Golubitsky, Stewart & Schaeffer (1989, Chapter XIX). In SG's (1989) experiment, a Hopf bifurcation of the Mb state, if it can be assumed to exist yet not to have been discovered, appears to be subcritical, rather than supercritical, because of the region G where pure (2, 3) and time-dependent states coexist. A method of determining the sub/supercriticality of the Hopf bifurcation is established in the Appendix using the centre manifold theorem and normal-form theory.

Figure 5 shows the schematic bifurcation diagram of stationary states for a typical case $\alpha = 1$. The thin solid curves in figure 5(*a*) ($\beta_1 > \beta_c$) and in figure 5(*a*, *c*) ($\beta_1 > \beta_d$) denote the lower and upper boundaries of the Mb state. In the rectangular case, SG (1989) observed neither the Ma nor Mb state. The Mb state in figure 5 is replaced by the coexistence of the S1 and S2 state (region C in figure 9 of SG 1989). Note that the $\mathrm{Ma}_{\pm}$ state in figure 5 exists far from point X, which is believed to be the reason why SG (1989) did not observe the Ma state in the rectangular case. The curve where the Ma and Mb states coincide is determined by substituting (3.7) into (3.15):

$$C_4: \quad A_0 = \left[\alpha^2 + \left\{\frac{D(\beta_1 + \beta_2)}{2(A_1 + C + D)}\right\}^2\right]^{\frac{1}{2}}, \tag{3.22}$$

FIGURE 6. Schematic bifurcation diagram for the rectangular case, with various fixed frequency offsets β_1. The horizontal axis denotes the forcing amplitude A_0. Thick and thin solid lines respectively show stable and unstable stationary states. A Hopf bifurcation from the Mb state is denoted as ⊕.

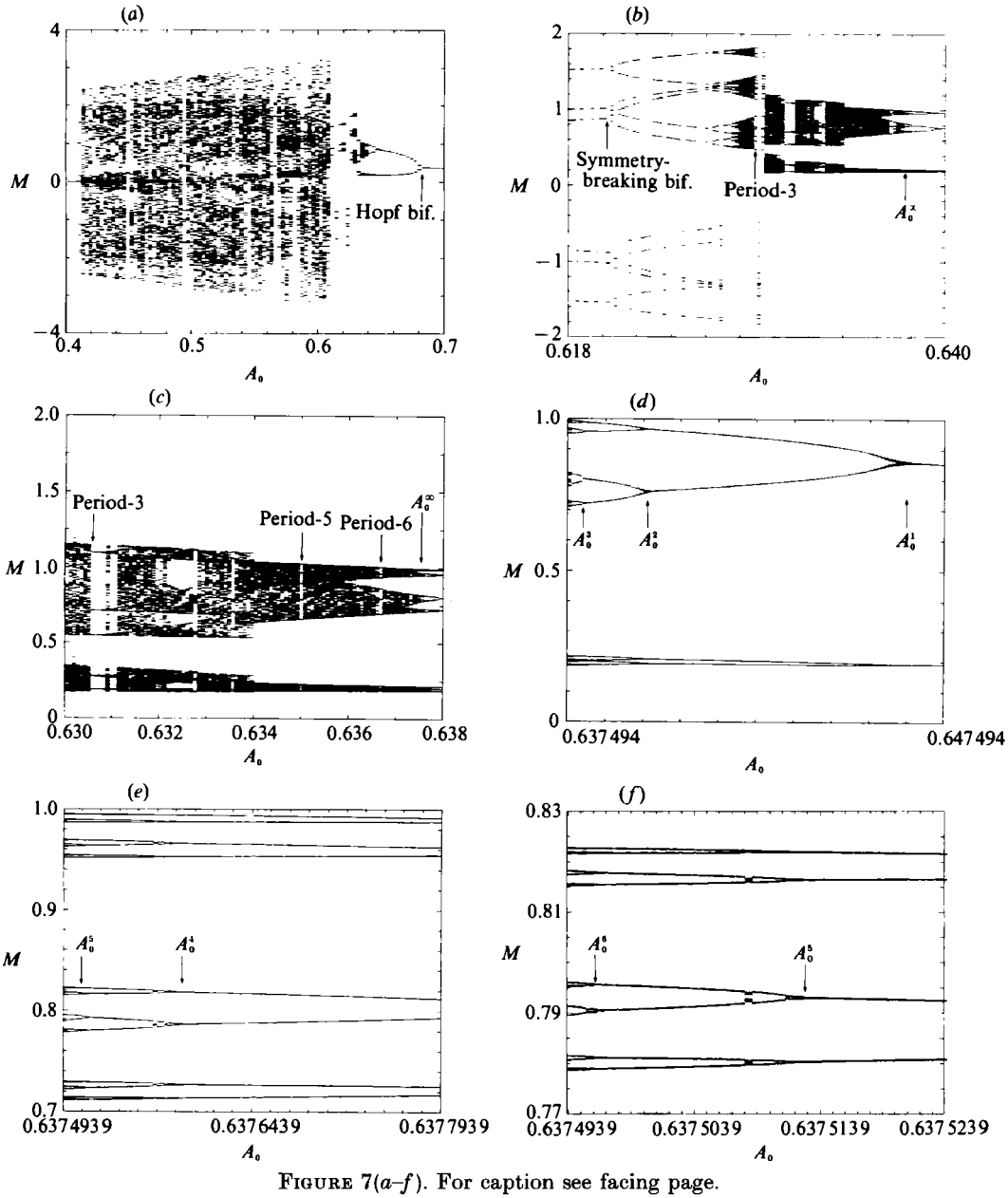

FIGURE 7(*a–f*). For caption see facing page.

with
$$\beta_1 > \beta_e \equiv \frac{2A_1+D}{2(A_1-C)}. \tag{3.23}$$

The fixed points and their classification of stabilities are listed in table 1. At $\beta_1 = \beta_f$ the bifurcation from S1 to Mb changes from supercritical to subcritical. Bifurcation diagrams for various fixed β_1 are shown in figure 6. Schematic phase-space structures shown by figure 10 of SG (1989), except for region C, are well reproduced in figure 6. The regions A, B, C, D of figures 9, 10 of SG (1989) correspond respectively to f, g, h (and l), m of figure 5. When $\beta_1 > \beta_b$, the Mb state bifurcating from S2 is also stable

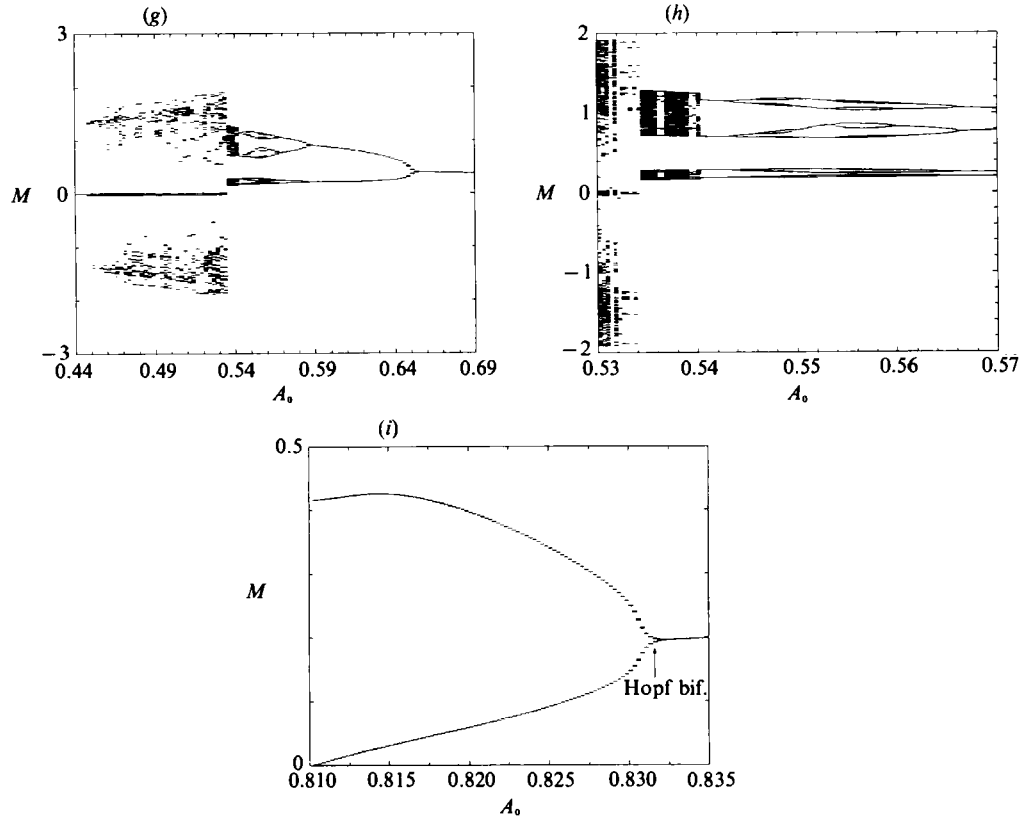

FIGURE 7. Numerical Poincaré plots of M at $\dot{q}_1 = 0$, with various forcing amplitudes A_0, a fixed frequency offset $\beta_1 = 0.6$ and nonlinear coefficients (3.16). The damping coefficient α is 0.1 (a–f), 0.2 (g, h) and 0.75 (i). A Hopf bifurcation from Mb is supercritical for all cases. The same initial conditions may settle down on the distinct symmetric attractors as A_0 varies. (d–f) Self-similar structure of period-doubling bifurcation.

because the bifurcating point lies on the stable branch of S2. (See figure 6; $\beta_b < \beta_1 < 1$.) Thus the Hopf bifurcation of the Mb state disappears and periodic or chaotic orbits vanish. When β_1 exceeds β_c, the multiplicity of the Mb state appears. Moreover, when $\beta_1 > \beta_e$, the bifurcation points of the Ma and Mb states on S1 swap order and a transcritical bifurcation point emerges.

The non-stationary-state bifurcation of the system presented, (3.1), with the coefficients of (3.16) was examined by a numerical calculation of bifurcation diagrams. Figure 7 shows Poincaré plots of M at $\dot{q}_1 = 0$, using various forcing amplitudes A_0 and other parameters fixed. The initial condition is chosen as $(\bar{p}_1, \bar{q}_1, \bar{p}_2, \bar{q}_2) + (0.01, 0, 0.01, 0)$ where an overbar denotes the Mb state. A frequency offset of 0.6 is present for β_1 and three typical damping coefficients were chosen: (a) $\alpha = 0.1$, (b) 0.2, and (c) 0.75. Case (c) corresponds to $2a_{0\,\min} = 120$ μm. The Hopf bifurcation of Mb is supercritical in all three cases, and additionally, when α exceeds a critical value (see case c), only periodic orbits appear in the time-dependent region.

Typical examples of numerically obtained orbits are shown in figure 8. The numerical integration was carried out by the fourth-order Runge–Kutta scheme, and $\Delta\tau$ is taken as 0.01. There exist at most four symmetric attractors resulting from the symmetry $(r_1, r_2) \to (-r_1, r_2)$, $(r_1, -r_2)$, $(-r_1, -r_2)$. The period-doubling bifurcation was examined numerically in detail and observed up to period 2^6 as well as periodic

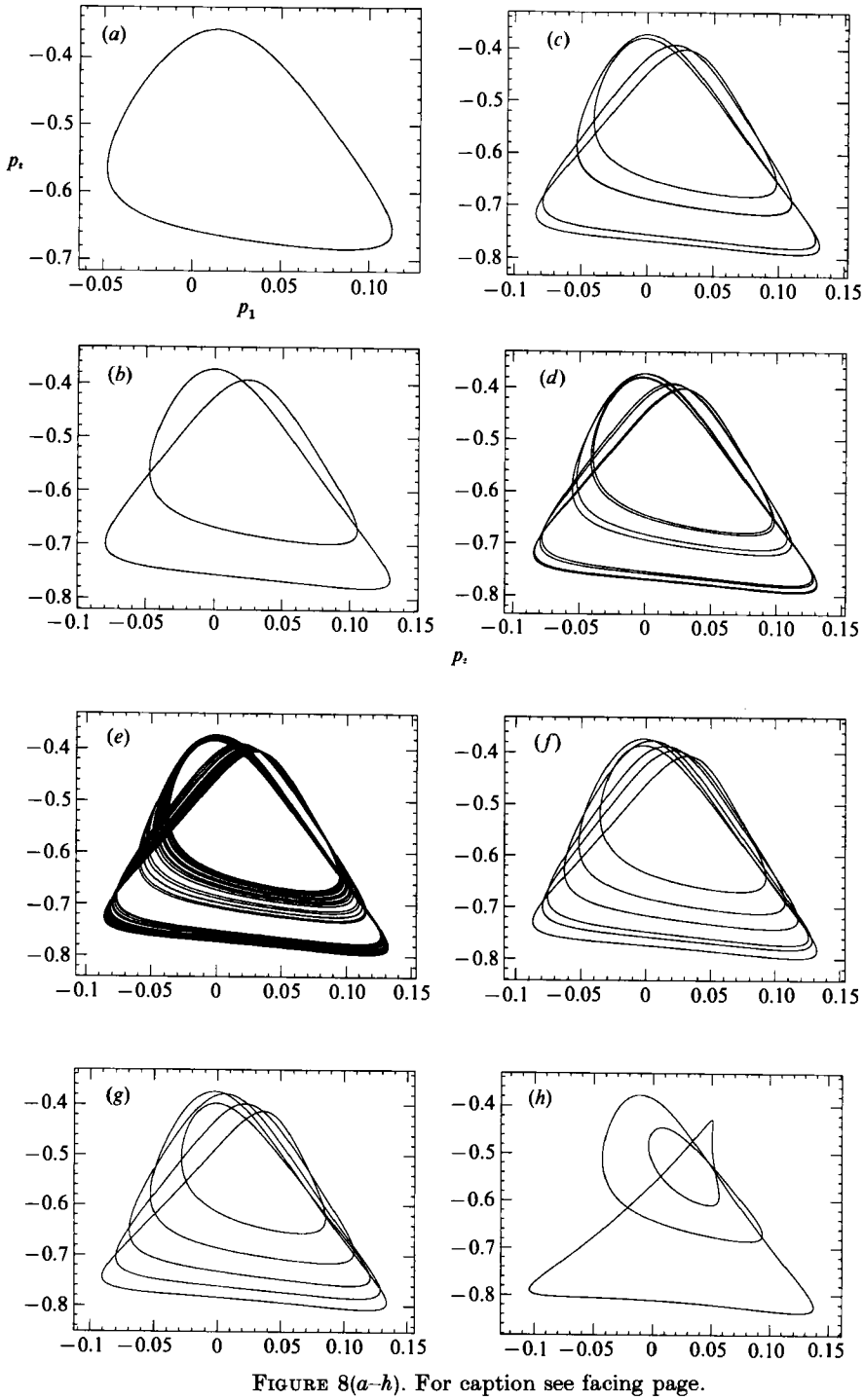

FIGURE 8(*a–h*). For caption see facing page.

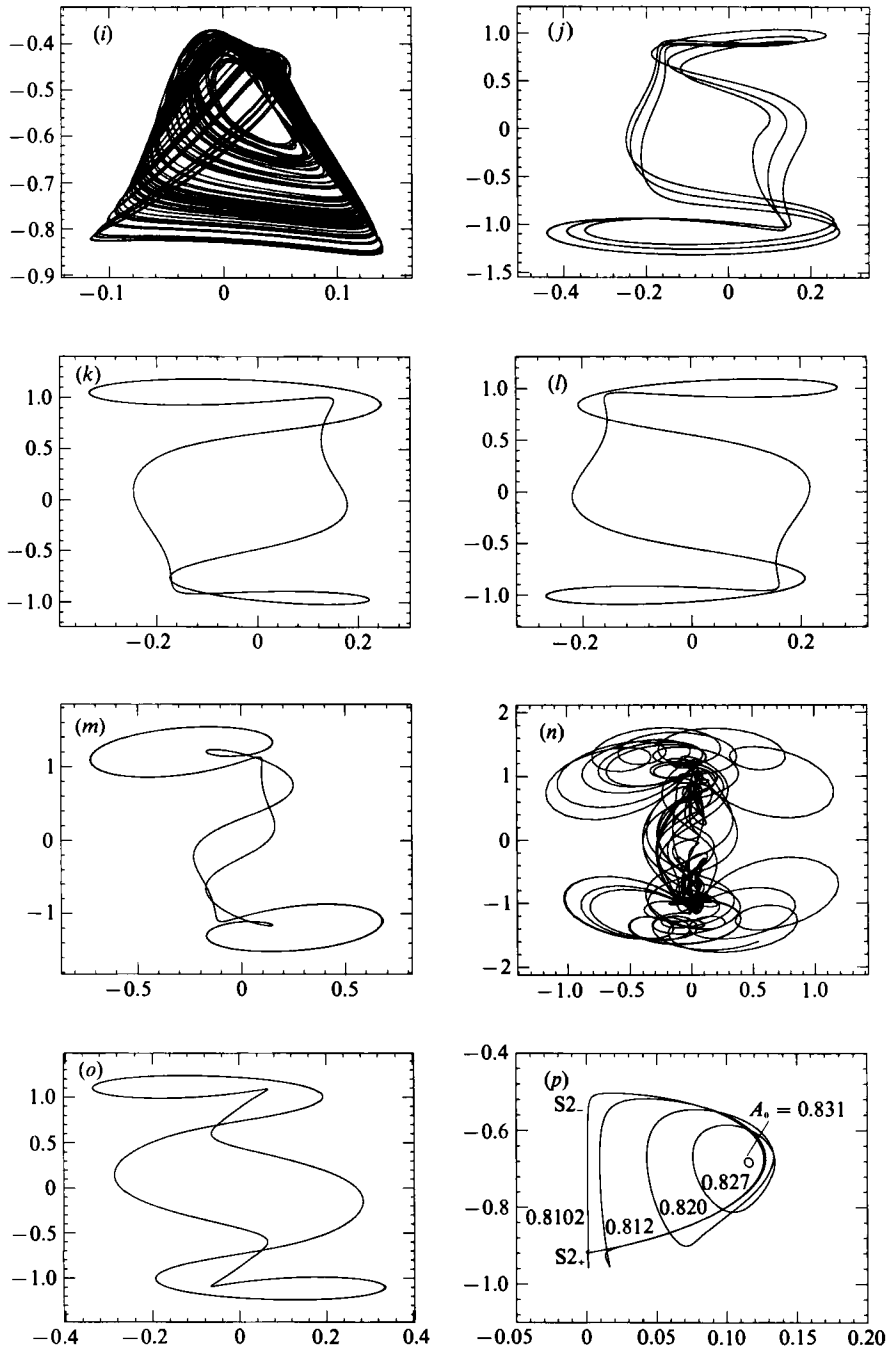

FIGURE 8. Numerical examples of the dynamical equations (3.1) with parameters (3.16), $\beta_1 = 0.6$, $\alpha = 0.1$ for (a–o), and $\alpha = 0.75$ for (p). Orbits are projected on the in-phase-amplitude (p_1, p_2)-plane. Note that p_1 and p_2 are proportional to the wave-mode amplitudes A_{32} and A_{23} of SG (1989). (a) $A_0 = 0.66$: periodic orbit with period-1, (b) 0.64: period-2, (c) 0.638: period-4, (d) 0.63775: period-8, (e) 0.637: chaos, (f) 0.6367: period-6, (g) 0.635: period-5, (h) 0.63065: period-3, (i) 0.63: chaos, (j) 0.629: period-3, (k) 0.622: period-1, (l) 0.618: period-1, (m) 0.566: period-1, (n) 0.5: chaos, (o) 0.448: period-1. The attractors (j), (k), (m) are asymmetric in the transformation $(r_1, r_2) \to (r_1, -r_2)$. ($p$) Periodic orbits approaching a homoclinic cycle. The single mode-2 stationary state is denoted by $S2_+$ and $S2_-$.

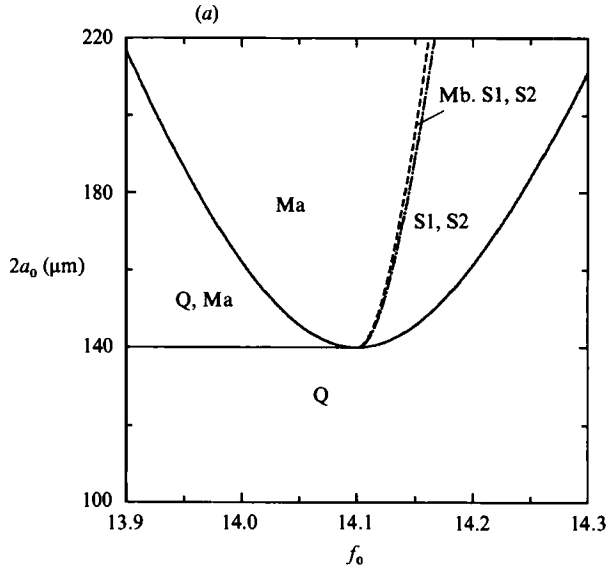

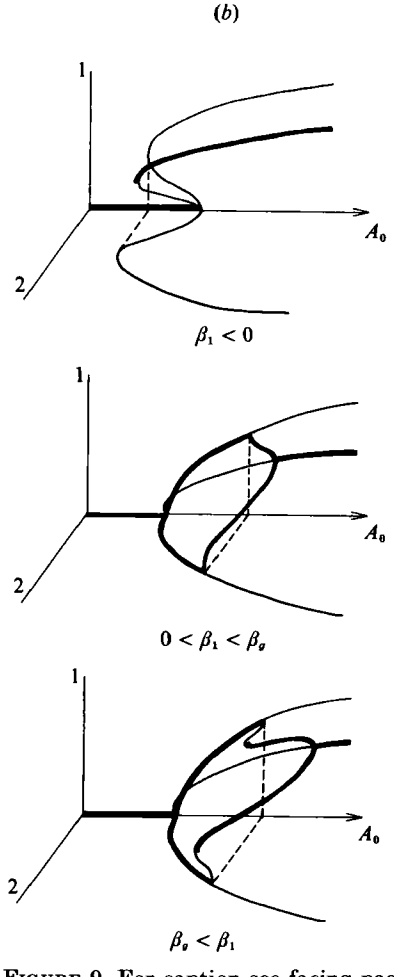

FIGURE 9. For caption see facing page.

windows containing period-3, -5, and -6 orbits. The bifurcation point of period-2^{n-1} to -2^n is denoted by A_0^n. The accumulation point was approximately $A_0^\infty = 0.6374963\ldots$. The Feigenbaum number defined by

$$\delta = \lim_{n\to\infty} \frac{A_0^n - A_0^{n-1}}{A_0^{n+1} - A_0^n}$$

was about 4.56 for $n = 5$, which was close to the universal constant 4.669... of the one-dimensional map. When A_0 is below 0.6295, a larger attractor appears where p_2 takes positive and negative values. The asymmetric attractor (k) with respect to $p_2 = q_2$ becomes symmetric in (l), which implies the symmetry-breaking (or symmetric saddle-node) bifurcation.

For $\alpha = 0.75$, a hysteresis is found where, for an initial condition near the Mb state, periodic orbits are obtained for A_0 below the stability curve for the zero solution. Moreover, as A_0 decreases, the computed period of the orbit increases, the periodic orbit approaches to a homoclinic cycle which consists of heteroclinic orbits connecting $S2_+$ and $S2_-$ and suddenly disappears (figure 8p). This type of bifurcation (homoclinic bifurcation) was observed by SG (1989) (figures 11 and 12). However, the appearance of the attractors presented here does not resemble theirs.

The Hopf bifurcation depends strongly on the nonlinear coefficients. In Kambe & Umeki (1990), the value -1.6, which was not the theoretically predicted one, was used for D instead of -0.8. In this case the Hopf bifurcation was subcritical and both periodic and chaotic attractors appeared with $2a_{0\min} = 120$ μm.

3.2. *Square case*

The bifurcation of two completely degenerate modes $(1,0)$ and $(0,1)$ in a square container was examined by Nagata (1989), who investigated the dependence on the depth of the coefficients A_1, C, D. Because the present study is focused on the relatively deep-water case, its square container case is included by Nagata (1989), who made no comparison with experiment, and the theoretical result of the bifurcation are similar to each other. Thus a brief comparison is made between the theoretical results and SG's (1989) experimental findings. Using $\beta_1 = \beta_2$, r_m of the Ma state is expressed as

$$r_{1\pm} = r_{2\pm} = \left\{\frac{-\beta_1 \pm (A_0^2 - \alpha^2)^{\frac{1}{2}}}{A_1 + C}\right\}^{\frac{1}{2}}.$$

Thus the region where the $Ma_\pm$ state exists is identical to $S1_\pm$ and $S2_\pm$ states. The Mb state satisfies the relation

$$2\beta_1 + (A_1 + C + D)(r_1^2 + r_2^2) = 0, \tag{3.24}$$

and exists if $\beta_1 > 0$. The bifurcation curves from the S1, S2 and Ma states are

$$A_0 = \left\{\alpha^2 + \left(\frac{(-A_1 + C + D)\beta_1}{A_1 + C + D}\right)^2\right\}^{\frac{1}{2}} \quad \text{for} \quad \text{S1, S2}, \tag{3.25}$$

FIGURE 9. (*a*) Theoretical parameter-space diagram corresponding to the square case (figure 4) of SG (1989). The signs denote stable fixed points. The regions of figure 4(*b*) of SG correspond as follows: A to Ma, Q, B to Ma, C to Mb and D to S1, S2. The bifurcation curves between Ma and Mb (broken curve) and between Mb and S1, S2 (dotted-dashed curve) exist in the region $f_0 > f_*$, although SG suggest that they are in the region $f_0 < f_*$. (*b*) Schematic bifurcation diagrams. Note that the diagrams are invariant under the exchange of S1 and S2, owing to the square geometry of the container.

and $$A_0 = \left\{\alpha^2 + \left(\frac{D\beta_1}{A_1+C+D}\right)^2\right\}^{\frac{1}{2}} \quad \text{for} \quad \text{Ma}. \tag{3.26}$$

The parameter-space and bifurcation diagrams are shown in figure 9. (See also figure 5 of Nagata 1989 and compare it with figure 9.) The multiplicity of Mb states appears when f_0 increases, but this is not drawn in figure 9. A third-order model predicts that the Ma state is stable for $f_0 < f_*$ and the bifurcations from the S1 and S2 states to the Ma state exist in the region $f_0 > \mathrm{F}_*$. SG (1989) show in their figure 4(*b*) that pure modes (S1 and S2 in the presented notation) and their bifurcation to mixed states (Ma) exist only in $f_0 < f_*$. The reason for this discrepancy which was not noted by Feng & Sethna (1989) is not still clear yet: however, fifth- or higher-order nonlinear terms may bend the bifurcation curves (3.25), (3.26) to the region $f_0 < f_*$. This difference certainly appears if the nonlinear coefficients are taken as satisfying the inequalities (3.17).

Using (3.1), the temporal evolution of the angular momentum is given by

$$\dot{M} = -2\alpha M + \{-\Delta\beta + (C-A_1)\,r_1^2 + (A_2-C)\,r_2^2\}\,(p_1 p_2 + q_1 q_2). \tag{3.27}$$

It should be noted that (3.27) has no forcing terms. When the system has circular symmetry ($A_1 = A_2 = C$) and complete degeneracy ($\beta_1 = \beta_2$), the angular momentum tends to vanish exponentially. This property also holds for the four-degree-of-freedom Hamiltonian system considered by Umeki & Kambe (1989). However, if the symmetry or the degeneracy breaks, the angular momentum can be maintained.

4. Homoclinic chaos in the average Hamiltonian system

Non-periodic mode competition of surface wave systems for the specific resonance condition was also considered for a conservative system (Holmes 1986) from the viewpoint that a small perturbation breaks the integrability of the Hamiltonian oscillation system. The present 2:1:2 external–internal Faraday resonance is studied using this idea. If the following two successive canonical transformations are selected:

$$(q_i, p_i) = ((2\hat{P}_i)^{\frac{1}{2}} \cos\hat{Q}_i, \quad (2\hat{P}_i)^{\frac{1}{2}} \sin\hat{Q}_i), \quad i = 1, 2, \tag{4.1}$$

$$\hat{Q}_1 = Q_1 + Q_2, \quad \hat{Q}_2 = Q_2, \quad \hat{P}_2 = P_2 - P_1, \quad \hat{P}_1 = P_1, \tag{4.2}$$

the dynamical equations (3.1*a–d*) can be put in the form

$$\dot{P}_1 = -2DP_1(P_2-P_1)\sin 2Q_1 - 2A_0 P_1 \sin 2(Q_1+Q_2) - 2\alpha P_1, \tag{4.3a}$$

$$\dot{Q}_1 = \Delta\beta + EP_1 + FP_2 - D(P_2-2P_1)\cos 2Q_1 - A_0\{\cos 2(Q_1+Q_2) - \cos 2Q_2\}, \tag{4.3b}$$

$$\dot{P}_2 = -2A_0\{P_1 \sin 2(Q_1+Q_2) + (P_2-P_1)\sin 2Q_2\} - 2\alpha P_2, \tag{4.3c}$$

$$\dot{Q}_2 = \beta_2 + 2A_2 P_2 + FP_1 - DP_1 \cos 2Q_1 - A_0 \cos 2Q_2, \tag{4.3d}$$

where $$E = 2(A_1+A_2-2C-D), \quad F = 2(C-A_2)+D, \tag{4.4a,b}$$

and the total Hamiltonian is given by

$$H = H_0 + H_1, \tag{4.5}$$

$$H_0 = \beta_1 P_1 + \beta_2(P_2-P_1) + A_1 P_1^2 + + A_2(P_2-P_1)^2 + (2C+D)\,P_1(P_2-P_1) - DP_1(P_2-P_1)\cos 2Q_1, \tag{4.6a}$$

$$H_1 = -A_0\{P_1 \cos 2(Q_1+Q_2) + (P_2-P_1)\cos 2Q_2\}. \tag{4.6b}$$

When there is no external forcing and damping ($A_0 = \alpha = 0$), this system has two conservative quantities, H_0 and P_2, and is integrable. The heteroclinic orbits in the (P_1, Q_1)-plane approaching $P_1 = 0$ lead to the relation

$$\cos 2Q_1 = \frac{\Delta\beta + FP_2 + \frac{1}{2}EP_1}{D(P_2 - P_1)}. \tag{4.7}$$

Here $D \neq 0$ is assumed. Thus the heteroclinic orbits connecting to the points $P_*: (P_1, Q_1) = (0, \frac{1}{2}\arccos[(\Delta\beta + FP_2)/DP_2])$ exist if

$$-1 < \frac{\Delta\beta + FP_2}{DP_2} < 1. \tag{4.8a}$$

Similarly for the orbits connecting $P_1 = P_2$, the condition is

$$-1 < \frac{\Delta\beta - FP_2}{DP_2} < 1. \tag{4.8b}$$

From (4.8), the following relation holds:

$$\dot{Q}_1 + \dot{Q}_2 = \beta_2 + (A_1 - A_2)P_1 + 2A_2P_2. \tag{4.9}$$

It should be noted that the system for the completely degenerate non-axisymmetric modes in a circular container has no heteroclinic orbits since $\Delta\beta = 0$ and $A_1 = A_2 = C$. The heteroclinic orbit connecting to the saddle point P_* is given by

$$P_1(\tau) = \pm 2P_1[D^2P_2^2 - (\Delta\beta + FP_2)^2 - \{2D^2P_2 + E(\Delta\beta + FP_2)\}P_1 + (D^2 - \tfrac{1}{4}E^2)P_1^2]^{\frac{1}{2}}, \tag{4.10}$$

$$Q_1(\tau) = \int_0^\tau \frac{\{\Delta\beta + (A_1 - A_2)P_2\}P_1}{P_2 - P_1}\,\mathrm{d}\tau + Q_{10}, \tag{4.11}$$

$$\begin{aligned} Q_2(\tau) &= \int_0^\tau \frac{-(A_1 - A_2)P_1^2 - (\beta_1 - 2A_2P_2)P_1 + (\beta_2 + 2A_2P_2)P_2}{P_2 - P_1}\,\mathrm{d}\tau + Q_{20} \\ &\equiv Q_2^*(\tau) + Q_{20}, \end{aligned} \tag{4.12}$$

Similar to Holmes (1986), a Poincaré map is considered on the cross-section $Q_2 =$ const. based on the reduction method, which assumes the existence of homoclinic orbits (strictly speaking, heteroclinic orbits in the (P_1, Q_1)-plane) and $\Omega = \partial H/\partial P_2 \neq 0$ in the neighbourhood of the homoclinic orbits. The first assumption can be satisfied if parameters are chosen so that (4.8*a*) or (4.8*b*) holds. In order to satisfy the second assumption, $\dot{Q}_2$, which can be expressed by $\dot{Q}_1, P_1$, etc. using (4.9) or its correspondent to the (4.8*b*), must remain of the same sign on the homoclinic orbit. These two assumptions give restrictions on the parameters appearing in the Hamiltonian.

When a small external forcing is added, homoclinic orbits becomes split and stable and unstable manifolds intersect transversally. This intersection brings Smale-horseshoe mapping and Cantor sets in the neighbourhood of perturbed homoclinic orbits (see Guckenheimer & Holmes 1986). Using the notation $y_\epsilon = (P_1, Q_1)$, the perturbed dynamical system (4.1) can be rewritten as

$$\dot{y}_\epsilon(\tau) = w_0(y_\epsilon, P_{2\epsilon}) + \epsilon w_1(y_\epsilon, P_{2\epsilon}, Q_{2\epsilon}), \tag{4.13a}$$

$$\dot{P}_{2\epsilon}(\tau) = \epsilon w_2(y_\epsilon, P_{2\epsilon}, Q_{2\epsilon}), \tag{4.13b}$$

$$\dot{Q}_{2\epsilon}(\tau) = Q(y_\epsilon, P_{2\epsilon}), \tag{4.13c}$$

where $$w_0 = \left(-\frac{\partial H_0}{\partial Q_1}, \frac{\partial H_0}{\partial P_1}\right), \quad \epsilon w_1 = \left(-\frac{\partial H_1}{\partial Q_1} - 2\alpha P_1, \frac{\partial H_1}{\partial P_1}\right), \quad \epsilon w_2 = \frac{\partial H_1}{\partial Q_2},$$

ϵ implies a small parameter of the forcing and damping and the subscript ϵ denotes the perturbed orbit. Here two small parameters ϵ and ϵ introduced towards the end of §2 should be distinguished. Here the forcing A_0 and damping α are small compared with $\Delta\beta$,although they are in the same order in the previous sections. The amount of splitting of stable and unstable manifolds is given by the Melnikov function

$$\bar{M}(P_{20}, Q_{20}) = n(y_0)\,[y_\epsilon^{\mathrm{u}} - y_\epsilon^{\mathrm{s}}]. \tag{4.14}$$

where $y_\epsilon^{\mathrm{u,s}}$ denotes the perturbed orbits on unstable and stable manifolds,

$$n(y_0) = \left(\frac{\partial H_0}{\partial P_1}, \frac{\partial H_0}{\partial Q_1}\right)$$

is (the (P_1, Q_1) components of) the normal to the unperturbed homoclinic orbit. The first variational equation gives

$$\bar{M}(P_{20}, Q_{20}) = \epsilon \int_{-\infty}^{\infty} [w_0 \wedge w_1 + w_0 \wedge \mathrm{D}_{P_2} w_0 I(\tau)]\,(y(\tau, P_{20}), P_{20}, Q_2^*(\tau, P_{20}) + Q_{20})\,\mathrm{d}\tau, \tag{4.15}$$

where the wedge product is defined as $a \wedge b = a_1 b_2 - a_2 b_1$, D_{P_2} denotes the P_2 derivative, and

$$I(\tau) = -\int_0^\tau w_2\,\mathrm{d}\tau.$$

Using the following relations:

$$w_0 \wedge \epsilon w_1 = \{H_0, H_1\}_{Q_1, P_1} + 2\alpha P_1 \frac{\partial H_0}{\partial P_1},$$

$$\epsilon I(\tau) = -\frac{H_1}{\Omega} + 2\alpha P_2 \tau,$$

$$\left(\{\}_{Q_1, P_1} \text{ denotes a Poisson bracket: } \{f, g\}_{Q_1, P_1} = \frac{\partial f}{\partial Q_1}\frac{\partial g}{\partial P_1} - \frac{\partial f}{\partial P_1}\frac{\partial g}{\partial Q_1}\right),$$

an explicit expression is obtained for the Melnikov function which includes the damping terms as

$$\bar{M}(P_{20}, Q_{20}) = 2A_0\{(I_{1\mathrm{s}} + I_{2\mathrm{s}} + I_{3\mathrm{s}}) \sin 2Q_{20} + (I_{1\mathrm{c}} + I_{2\mathrm{c}} + I_{3\mathrm{c}}) \cos 2Q_{20}\} + 2\alpha(I_4 + I_5), \tag{4.16}$$

where

$$I_{1\mathrm{c}} = \int_{-\infty}^{\infty} -DP_1(P_2 - P_1)\,(\sin 2Q_2^* + \sin 2Q_1 \cos 2Q_2^*)\,\mathrm{d}\tau, \tag{4.17a}$$

$$I_{1\mathrm{s}} = \int_{-\infty}^{\infty} -DP_1(P_2 - P_1)\,(\cos 2Q_2^* - \sin 2Q_1 \sin 2Q_2^*)\,\mathrm{d}\tau, \tag{4.17b}$$

$$I_{2\mathrm{c}} = \int_{-\infty}^{\infty} \{\Delta\beta + EP_1 + FP_2 + DP_1 \cos 2Q_1\} P_1 \sin 2(Q_1 + Q_2^*)\,\mathrm{d}\tau, \tag{4.17c}$$

$$I_{2\mathrm{s}} = \int_{-\infty}^{\infty} \{\Delta\beta + EP_1 + FP_2 + DP_1 \cos 2Q_1\} P_1 \cos 2(Q_1 + Q_2^*)\,\mathrm{d}\tau, \tag{4.17d}$$

$$I_{3\mathrm{c}} = \int_{-\infty}^{\infty} DP_1 \sin 2Q_1 \{\Delta\beta + (E + F)\,P_1 + DP_1 \cos 2Q_1\} \times \{P_1 \cos 2(Q_1 + Q_2^*) + (P_2 - P_1) \cos 2Q_2^*\}/\Omega\,\mathrm{d}\tau, \tag{4.17e}$$

$$I_{3s} = \int_{-\infty}^{\infty} DP_1 \sin 2Q_1 \{\Delta\beta + (E+F)P_1 + DP_1 \cos 2Q_1\}$$
$$\times \{-P_1 \sin 2(Q_1+Q_2^*) - (P_2-P_2)\sin 2Q_2^*\}/\Omega \, d\tau, \quad (4.17f)$$

$$I_4 = \int_{-\infty}^{\infty} \{\Delta\beta + EP_1 + FP_2 + D(2P_1-P_2)\cos 2Q_1\} P_1 \, d\tau, \quad (4.17g)$$

$$I_5 = -\int_{-\infty}^{\infty} DP_1 \sin 2Q_1 \{\Delta\beta + (E+F)P_1 + D P_1 \cos 2Q_1\} P_2 \tau \, d\tau. \quad (4.17h)$$

Thus the Melnikov function has simple zeros if $0 \leqslant \alpha \ll A_0$. This implies the existence of uncountable non-periodic orbits as well as countable many periodic orbits. These expressions can be simplified if P_1, Q_1, Q_2^* are even or odd functions with respect to τ.

The following three cases were considered as examples:

Case (*a*): $A_1 = A_2 = C = -3, \quad D = -4, \quad P_2 = 0.25, \quad \beta_1 = 0, \quad \beta_2 = -1,$ (4.18)

Case (*b*): $A_1 = A_2 = D = 2, \quad C = 1, \quad P_2 = 1.0, \quad \beta_1 = \beta_2 = 0,$ (4.19)

Case (*c*): $A_1 = A_2 = C = D = 1, \quad P_2 = 1.0, \quad \beta_1 = \beta_2 = 0.$ (4.20)

A nearly degenerate case (*a*) possesses a homoclinic orbit expressed as

$$P_1(\tau) = \tfrac{1}{8}\operatorname{sech}\tau,$$
$$Q_1(\tau) = 2\arctan(e^{\tau}),$$
$$Q_2(\tau) = -Q_1(\tau) + (\beta_2 + 2A_2P_2)\tau + \tfrac{1}{2}\pi + Q_2(0).$$

Case (*b*) represents the completely degenerate mode-pair and heteroclinic orbits:

$$P_1(\tau) = \frac{e^{4\tau}}{1+e^{4\tau}}, \quad Q_1(\tau) = Q_1(0).$$

Complete degeneracy with circular symmetry is exemplified by case (*c*), which has no homoclinic or heteroclinic orbits. The numerically obtained Poincaré sections are shown in figure 10. The forcing is taken as $A_0 = 0.2$. The initial conditions are chosen to take the same value of the perturbed Hamiltonian as in case (*a*) and $P_1(0) = 0.5$, $Q_1(0) = 2\pi/50, 4\pi/50, \ldots, 2\pi$, $Q_2(0) = 0$. Stochastic layers are found in case (*a*) and (*b*), but not in (*c*).

The experimentally observed mode competition of surface waves in a (small) container is considered as a motion on a strange attractor. It was found that the condition $\Omega \neq 0$ did not hold for the numerically computed strange attractors drawn in figure 7. This implies that the mathematical proof of homoclinic chaos of a Hamiltonian system does not necessarily apply to the observed mode competitions of surface waves. It should be stressed, however, that both Hamiltonian and dissipative surface-wave systems can possess chaotic motions when the degeneracy or the circular symmetry breaks.

5. Conclusion

A theoretical analysis of the subharmonic response of two resonant modes of surface waves in rectangular and square containers is made based on the third-order nonlinear dynamical system derived by the average Lagrangian method. Estimates

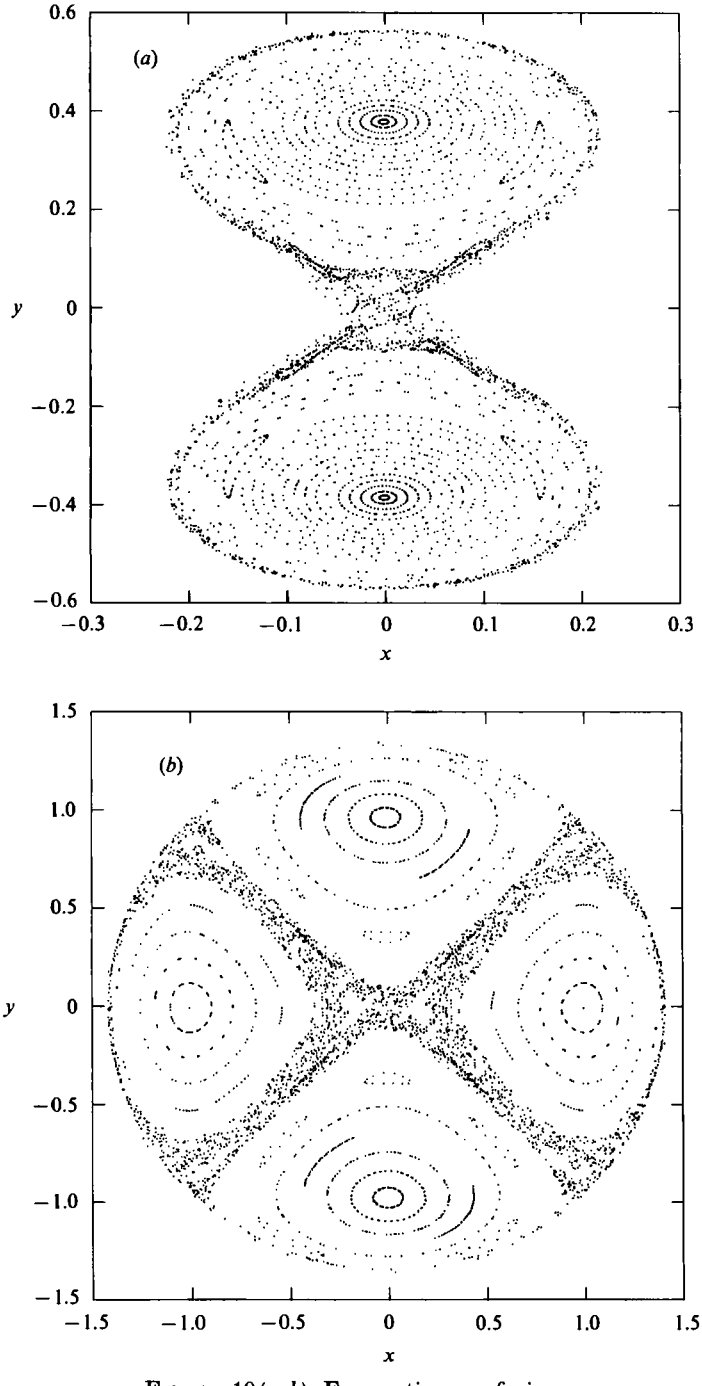

FIGURE 10(*a*, *b*). For caption see facing page.

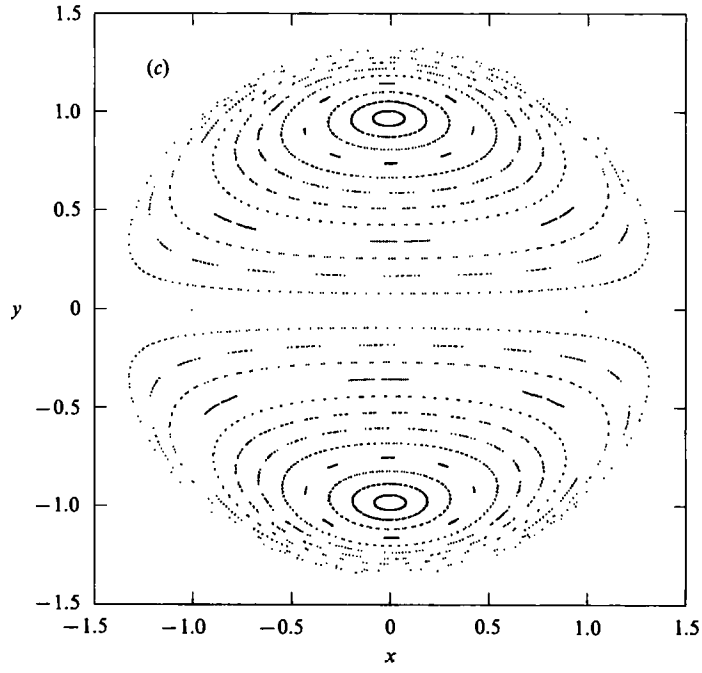

FIGURE 10. Two-dimensional projection of a Poincaré map with respect to $Q_2 = 0 \pmod{2\pi}$ on the $(x, y) = ((2P_1)^{\frac{1}{2}} \cos Q_1, (2P_1)^{\frac{1}{2}} \sin Q_1)$ plane. (*a*): nearly degenerate case; (*b*): completely degenerate case; (*c*) completely degenerate and circular-symmetric case. In (*a*), the initial conditions are chosen on the same level surface $H = \text{const.}$

of nonlinear coefficients are made for some typical case including capillarity. The previous results for gravity waves obtained by the perturbation expansion method are reproduced. The two different methods are confirmed to lead the same results up to the third-order nonlinearity. The formula for coefficients is applied to the experiment of Simonelli & Gollub (1989) and the bifurcations of stationary states are examined. The similarities and differences between the theoretical results obtained by the third-order nonlinear model and the experimental findings by SG (1989) are clarified. It is shown that the periodic mode competition occurs from a Hopf bifurcation, which is supercritical for the predicted nonlinear coefficients of gravity waves but may become subcritical for slightly modified values of the coefficients, of a mixed rotating wave (Mb) state for the slightly rectangular case. If the damping coefficient α is sufficiently small, the periodic orbits in the phase space bifurcate into the complicated orbits. The stable stationary states are shown in the parameter space of the amplitude and the frequency of the external forcing. The theoretical diagram includes a mixed rotating wave (Mb) state, which was not observed by SG (1989), and the region for Mb is replaced by a region of coexistence of two single modes.

Bifurcations from single (pure) modes to a mixed modes in a square container are obtained. The theoretical diagram for a square container show bifurcations in the region $f_0 > f_*$; on the other hand SG (1989) shows them in $f_0 < f_*$.

The existence of transversal intersection of homoclinic orbits in the present average Hamiltonian system with suitable parameters is shown based on the Melnikov's method. The homoclinic chaos is demonstrated numerically. The relation

between homoclinic chaos in the conservative system and strange attractors in the strongly dissipative system is discussed. The rigorous proof of homoclinic chaos does not directly apply to the strongly dissipative system, as is observed by the experiment in a container, since the assumption for the reduction method is not satisfied.

Finally, two advantages of Miles' average Lagrangian formulation to the perturbation expansion method are stressed. First, an explicit Hamiltonian structure of mode interactions is obtained as well as the external forcing and capillarity. Second, extension of the system to involve more than three internally resonant modes appears to be easy.

The author would like to thank Professor John W. Miles for critical comments and invaluable advice on his manuscripts, and for allowing him to recheck Miles' previous results. He is also grateful to Professor Funakoshi for useful discussions.

Appendix. Determination of the sub/supercriticality of the Hopf bifurcation

A theoretical analysis in §3 shows that the mode competition of surface waves originates in the Hopf bifurcation is described using the calculation of the centre manifold. This calculation may be particularly important when the effect of higher nonlinearity on the Hopf bifurcation is discussed.

First we rewrite the system (3.1) in the form

$$\dot{z}_i = -\alpha z_i + T_{ij}\frac{\partial H}{\partial z_j}, \tag{A 1}$$

where the repeated indices imply summation, and the variables are

$$(z_1, z_2, z_3, z_4) = (p_1, p_2, q_1, q_2). \tag{A 2}$$

The 4×4 matrix T_{ij} is defined by

$$T_{ij} = \begin{cases} -1 & \text{if} \quad (i,j) = (1,3),(2,4), \\ 1 & \text{if} \quad (i,j) = (3,1),(4,2), \\ 0 & \text{otherwise}, \end{cases} \tag{A 3}$$

and the Hamiltonian function is expressed as

$$H = H_{\mathrm{L}} + H_{\mathrm{N}}, \tag{A 4}$$

$$H_{\mathrm{L}} = c_{ij} z_i z_j, \quad H_{\mathrm{N}} = c_{ijkl} z_i z_j z_k z_l. \tag{A 5), (A 6}$$

The coefficients c_{ij} and c_{ijkl}, which are symmetric in all subscripts, are given by

$$c_{ij} = \begin{cases} \frac{1}{2}(\beta_i + A_0) & \text{if} \quad i = j = 1,2, \\ \frac{1}{2}(\beta_{i-2} - A_0) & \text{if} \quad i = j = 3,4, \\ 0 & \text{otherwise}, \end{cases} \tag{A 7}$$

and

$$c_{ijkl} = \begin{cases} \frac{1}{4}A_1 & \text{if } (i,j,k,l) = (1,1,1,1) \text{ and } (3,3,3,3), \\ \frac{1}{4}A_2 & \text{if } (i,j,k,l) = (2,2,2,2) \text{ and } (4,4,4,4), \\ \frac{1}{12}A_1 & \text{if } (i,j,k,l) = (1,1,3,3),(1,3,1,3),\ldots,(3,3,1,1), \\ \frac{1}{12}A_2 & \text{if } (i,j,k,l) = (2,2,4,4),\ldots,(4,4,2,2), \\ \frac{1}{12}C & \text{if } (i,j,k,l) = (1,1,2,2),\ldots,(2,2,1,1),(3,3,4,4), \\ & \quad \ldots,(4,4,3,3), \\ \frac{1}{12}(C+D) & \text{if } (i,j,k,l) = (1,1,4,4),\ldots,(4,4,1,1),(2,2,3,3), \\ & \quad \ldots,(3,3,2,2), \\ -\frac{1}{24}D & \text{if } (i,j,k,l) = (1,2,3,4),\ldots,(4,3,2,1), \\ 0 & \text{if otherwise.} \end{cases} \tag{A 8}$$

Second, denoting by $\bar{p}_i$ the Mb state which is solved by the method in §3, we transform variables so that the origin coincides with Mb:

$$z_i = p_i + \bar{p}_i. \tag{A 9}$$

Substituting (A 9) into the Hamiltonian (A 4), and using the symmetry of the coefficients c_{ijkl}, we obtain

$$H = \tilde{H}_{\mathrm{L}} + \tilde{H}_{\mathrm{N}}, \tag{A 10}$$

$$\tilde{H}_{\mathrm{L}} = c_{ij}p_ip_j + 6c_{ijkl}\bar{p}_k\bar{p}_lp_ip_j, \tag{A 11}$$

$$\tilde{H}_{\mathrm{N}} = c_{ijkl}p_ip_jp_kp_l + 4c_{ijkl}\bar{p}_lp_ip_jp_k. \tag{A 12}$$

Constant and linear terms can be omitted in the Hamiltonian. The dynamical equations are described as

$$\dot{p}_i = -\alpha p_i + T_{ij}\frac{\partial H}{\partial p_j}, \tag{A 13}$$

where

$$\frac{\partial H}{\partial p_j} = F^1_{jk}p_k + F^2_{jkl}p_kp_l + F^3_{jklm}p_kp_lp_m, \tag{A 14}$$

$$F^1_{jk} = 2c_{jk} + 12_{jklm}\bar{p}_l\bar{p}_m, \quad F^2_{jkl} = 12c_{jklm}\bar{p}_m, \quad F^3_{jklm} = 4c_{jklm}. \tag{A 15), (A 16), (A 17}$$

In the Hamiltonian case ($\alpha = 0$), there is a property of the Jacobian matrix $\mathbf{\Pi}$ of (A 13) whose component is defined by $\Pi_{ij} = \partial\dot{p}_i/\partial p_j$. That is, if λ is an eigenvalue of $\mathbf{\Pi}$, then so are $\bar{\lambda}$, $-\lambda$, and $-\bar{\lambda}$ where an overbar denotes the complex conjugate. This property leads to the Jacobian matrix of the non-Hamiltonian case ($\alpha \neq 0$) having eigenvalues $\lambda-\alpha$, $\bar{\lambda}-\alpha$, $-\lambda-\alpha$, and $\bar{\lambda}-\alpha$, because damping terms with a common coefficient only shift the eigenvalues to the real negative side.

When the Mb state looses its stability, one of the eigenvalues must cross the imaginary axis. If the eigenvalue is real, the bifurcation implies another branch of stationary states. Because there are no such branches, the eigenvalue must be pure imaginary, and the above property implies that there are a pure imaginary pair ($\pm\mathrm{i}\omega$) and a complex pair ($-2\alpha\pm\mathrm{i}\omega$). Here the real part -2α comes from the fact that the total sum of the eigenvalues must be -4α.

Third, we perform a standard-form transform so that the linear part of (A 13) is represented in a block-diagonal form. Rewriting the system (A 13) into the form

$$\dot{p}_i = \tilde{A}_{ij}p_j + P_i, \tag{A 18}$$

where $\tilde{A}_{ij}p_j$ and P_i denote respectively linear and nonlinear terms, we transform p_i into x_i as

$$p_i = \tilde{B}_{ij}x_j. \tag{A 19}$$

The 4×4 transform matrix $\tilde{B}_{ij}$ satisfies the relation

$$\tilde{A}_{ik}\tilde{B}_{kj} = \tilde{B}_{ik}\tilde{C}_{kj} \tag{A 20}$$

and the 4×4 block-diagonal matrix $\tilde{C}_{ij}$ is

$$\tilde{C}_{ij} = \begin{pmatrix} C_1 & 0 \\ 0 & C_2 \end{pmatrix}, \quad C_1 = \begin{pmatrix} 0 & -\omega \\ \omega & 0 \end{pmatrix}, \quad C_2 = \begin{pmatrix} -2\alpha & -\omega \\ \omega & -2\alpha \end{pmatrix}. \tag{A 21), (A 22}a, b)$$

The equations for the new variables x_i are given by

$$\dot{x}_i = \tilde{C}_{ij}x_i + \tilde{X}_i \tag{A 23}$$

where nonlinear term $\tilde{X}_i$ is

$$\tilde{X}_i = \tilde{B}^{-1}_{ii'}T_{i'j'}F^2_{j'l'm'}\tilde{B}_{l'l}\tilde{B}_{m'm}x_l x_m + \tilde{B}^{-1}_{ii'}T_{i'j'}F^2_{j'l'm'n'}\tilde{B}_{l'l}\tilde{B}_{m'm}\tilde{B}_{n'n}x_l x_m x_n. \tag{A 24}$$

Moreover, rewriting the variables as $(x_1, x_2, x_3, x_4) = (x_1, x_2, y_1, y_2)$, or simply $= (x, y)$, the system becomes

$$\dot{x}_i = C_{1ij}x_j + f_i(x, y), \tag{A 25}$$

$$\dot{y}_i = C_{2ij}y_j + G_i(x, y), \tag{A 26}$$

where $f(0,0) = g(0,0) = 0$ along with its derivatives.

Since we are considering the Hopf bifurcation point with codimension-1 of the four-dimensional system, the centre manifold theorem implies that there exist two-dimensional stable and centre manifolds of the Mb state which are respectively tangent to the $x_1 = x_2 = 0$ and $y_1 = y_2 = 0$ plane. Thus we may approximate locally the centre manifold as a quadratic function of x_1, x_2 as

$$y_l = h^l(x) \equiv h^l_{ij}x_i x_j + O(x^3). \tag{A 27}$$

The local flow close to the Mb state is equivalent to the system

$$\dot{x}_i = C_{1ij}x_j + f_i(x, h(x)), \quad \dot{y}_i = C_{2ij}y_j. \tag{A 28), (A 29)}$$

In order to determine the sub/supercriticality of the Hopf bifurcation of (A 28), the second- and third-order nonlinearity of $f_i(x, h(x))$ is sufficient. For a detailed discussion, see Guckenheimer & Holmes (1985, §§3.2–3.4). Owing to $y = O(x^2)$, the necessary nonlinear terms are

$$f_l(x, y) = f^{l;xx}_{ij}x_i x_j + f^{l;xy}_{ij}x_i y_j + f^{l;xxx}_{ijk}x_i x_j x_k, + O(x^4), \tag{A 30}a$$

$$g_l(x, y) = g^{l;xx}_{ij}x_i x_j + O(x^3), \tag{A 30}b$$

where

$$f^{l;xx}_{ij} = B^{-1}_{li'}T_{i'j'}F^2_{j'l'm'}B_{l'i}B_{m'j}, \tag{A 31}$$

$$f^{l;xy}_{ij} = 2B^{-1}_{li'}T_{i'j'}F^2_{j'l'm'}B_{l'i}B_{m'j+2}, \tag{A 32}$$

$$f^{l;xxx}_{ijk} = B^{-1}_{li'}T_{i'j'}F^3_{j'l'm'n'}B_{l'i}B_{m'j}B_{n'k}, \tag{A 33}$$

$$g^{l;xx}_{ij} = B^{-1}_{l+2i'}T_{i'j'}F^2_{j'l'm'}B_{l'i}B_{m'j}, \quad \text{for} \quad l, i, j, k = 1, 2. \tag{A 34}$$

The coefficients $f^{l;xx}_{ij}, g^{l;xx}_{ij}, f^{l;xxx}_{ijk}$ and h^l_{ij} are symmetric in all subscripts, but $f^{l;xy}_{ij}$ is not. Substituting (A 27) into (A 26), using the chain rule and keeping $O(x^2)$ terms, we obtain

$$2h^l_{ki}x_i C_{1kj}x_j = C_{2lk}h^k_{ij}x_i x_j + g^{l;xx}_{ij}x_i x_j. \tag{A 35}$$

Symmetrizing the coefficient of $x_i x_j$ on the left-hand side of (A 35), we obtain the relation to be solved for h^l_{ij}:

$$h^l_{ki} C_{1kj} + h^l_{kj} C_{2ki} - C_{2lk} h^k_{ij} = g^{l,xx}_{ij}. \tag{A 36}$$

Using the notation $(h^l_1, h^l_2, h^l_3) = (h^l_{11}, h^l_{12}, h^l_{22})$ and the same notation for g^l_{ij}, (A 36) becomes

$$\tilde{D}_{ij} h^1_j + \omega h^2_i = g^1_i, \quad \omega h^1_i + \tilde{D}_{ij} h^2_j = g^2_i, \tag{A 37a, b}$$

where $\tilde{D}_{ij}$ is a 3×3 matrix defined by

$$\tilde{D}_{ij} = \begin{pmatrix} 2\alpha & 2\omega & 0 \\ -\omega & 2\alpha & \omega \\ 0 & -2\omega & 2\alpha \end{pmatrix}. \tag{A 38}$$

Using the values h^l_{ij} which can be obtained by solving (A 37), the $x_i y_j$ term in (A 30) is expressed as

$$f^{l,xy}_{ij} x_i y_j = \tfrac{1}{3}(f^{l,xy}_{im} h^m_{jk} + f^{l,xy}_{jm} h^m_{ki} + f^{l,xy}_{km} h^m_{ij})\, x_i x_j x_k, \tag{A 39}$$

where the coefficient is symmetrized again. The nonlinear terms in (A 25) are approximated up to $O(x^3)$ as

$$f_l(x, h(x)) = f^{l,2}_{ij} x_i x_j + f^{l,3}_{ijk} x_i x_j x_k, \tag{A 40}$$

where

$$f^{l,2}_{ij} = f^{l,xx}_{ij}, \tag{A 41}$$

$$f^{l,3}_{ijk} = f^{l,xxx}_{ijk} + \tfrac{1}{3}(f^{l,xy}_{im} h^m_{jk} + f^{l,xy}_{jm} h^m_{ki} + f^{l,xy}_{km} h^m_{ij}). \tag{A 42}$$

The normal-form theory means that the system (A 28) can be reduced in polar coordinates to

$$\dot{r} = \hat{a} r^3 + O(r^5), \quad \dot{\theta} = \omega + \hat{b} r^2 + O(r^4). \tag{A 43), (A 44}$$

The normal-form coefficient $\hat{a}$ is calculated by the coefficients (A 41), (A 42) as

$$\hat{a} = \tfrac{1}{8}\left[3(f^{1,3}_{111} + f^{1,3}_{122} + f^{2,3}_{112} + f^{2,3}_{222}) + \frac{2}{\omega}\{f^{1,2}_{12}(f^{1,2}_{11} + f^{1,2}_{22}) - f^{2,2}_{12}(f^{2,2}_{11} + f^{2,2}_{22}) - f^{1,2}_{11} f^{2,2}_{11} + f^{1,2}_{22} f^{2,2}_{22}\}\right], \tag{A 45}$$

which is equivalent to the formula (3.4.11) in Guckenheimer & Holmes (1986). The calculated value of $\hat{a}$ is negative for the case (3.16) and the values of α and β used in §3 and it implies that the Hopf bifurcation is supercritical.

Now the effect of higher nonlinearity on the Hopf bifurcation is discussed. The fifth-order nonlinearity is introduced in the Hamiltonian (A 4)

$$H_6 = c_{ijklmn} z_i z_j z_k z_l z_m z_n, \tag{A 46}$$

where the coefficient c_{ijklmn} is $O(\epsilon^2)$. There are two kinds of modification of the normal-form coefficient $\hat{a}$. One is a shift of the Mb state $\bar{p}_i$. The other is the appearance in the dynamical equation (A 13) of additional terms:

$$F^1_{ij} \to F^1_{ij} + 15 c_{ijklmn} \bar{p}_k \bar{p}_l \bar{p}_m \bar{p}_n, \tag{A 47}$$

$$F^2_{ijk} \to F^2_{ijk} + 20 c_{ijklmn} \bar{p}_l \bar{p}_m \bar{p}_n, \tag{A 48}$$

$$F^3_{ijkl} \to F^3_{ijkl} + 15 c_{ijklmn} \bar{p}_m \bar{p}_n. \tag{A 49}$$

Because these two modifications are $O(\epsilon^2)$, the effect of higher nonlinearity on $\hat{a}$ is also $O(\epsilon^2)$, and does not change the sign of $\hat{a}$ if the expansion parameter is sufficiently small. This ensures that, when the parameters are close to the codimension-2 bifurcation point X, the third-order nonlinear theory explain the periodic motion

well because $\hat{a}$ is positive. In fact, as β_1 tends to 0.5, both ω and coefficients $f_{ij}^{\ell,m}$ tend to zero, but their ratios remain finite. As the parameters go far from X, however the sign of $\hat{a}$ may change. When $\hat{a}$ is positive, the coefficients of r^5 in (A 43) should be calculated in order to obtain a finite-amplitude periodic orbit.

REFERENCES

Benjamin, T. B. & Ursell, F. 1954 The stability of the plane free surface of a liquid in vertical periodic motion. *Proc. R. Soc. Lond.* A **225**, 505–517.

Ciliberto, S. & Gollub, J. P. 1985 Chaotic mode competition is parametrically forced surface waves. *J. Fluid Mech.* **158**, 381–398.

Crawford, J. D., Knobloch, E. & Riecke, H. 1990 Period-doubling mode interactions with circular symmetry. *Physica* D **44**, 340–396.

Feng, Z. C. & Sethna, P. R. 1989 Symmetry-breaking bifurcations in resonant surface waves. *J. Fluid Mech.* **199**, 495–518.

Funakoshi, M. & Inoue, S. 1988 Surface waves due to resonant horizontal oscillation. *J. Fluid Mech.* **192**, 219–247.

Golubitsky, M., Stewart, I. & Schaeffer, D. G. 1989 *Singularities and Groups in Bifurcation Theory*, vol. 2. Springer.

Guckenheimer, J. & Holmes, P. 1986 *Nonlinear Oscillations, Dynamical Systems, and Bifurcations of Vector Fields*, 2nd edn. Springer.

Holmes, P. 1986 Chaotic motions in a weakly nonlinear model for surface waves. *J. Fluid Mech.* **162**, 365–388.

Kambe, T. & Umeki, M. 1990 Nonlinear dynamics of two-mode interactions in parametric excitation of surface waves. *J. Fluid Mech.* **212**, 373–393.

Karatsu, M. 1988 Nonlinear resonance and chaos of surface waves of water. Master's thesis, University of Tokyo (in Japanese).

Mack, L. R. 1962 Periodic, finite amplitude, axisymmetric gravity waves. *J. Geophys. Res.* **67**, 829–843.

Meron, E. & Procaccia, I. 1986 Low-dimensional chaos in surface waves: Theoretical analysis of an experiment. *Phys. Rev.* A **34**, 3221–3237.

Meron, E. & Procaccia, I. 1989 Reply to Miles. *Phys. Rev. Lett.* **63**, 1437.

Miles, J. W. 1976 Nonlinear surface waves in a closed basin. *J. Fluid Mech.* **75**, 419–448.

Miles, J. W. 1984*a* Nonlinear Faraday resonance. *J. Fluid Mech.* **146**, 285–302.

Miles, J. W. 1984*b* Internally resonant surface waves in a circular cylinder. *J. Fluid Mech.* **149**, 1–14.

Miles, J. W. 1989 Symmetries of internally resonant, parametrically excited surface waves. *Phys. Rev. Lett.* **63**, 1436.

Nagata, M. 1989 Nonlinear Faraday resonance in a box with a square base. *J. Fluid Mech.* **209**, 265–284.

Nobili, M., Ciliberto, S., Loccaiaro, B., Faetti, S. & Fronzoni, L. 1988 Time-dependent surface waves in a horizontally oscillating container. *Europhys. Lett.* **7**, 587–592.

Silber, M. & Knobloch, E. 1988 Parametrically excited surface waves in square geometry. *Phys. Lett.* **137**, 349–354.

Simonelli, F. & Gollub, J. P. 1989 Surface wave mode interactions: effect of symmetry and degeneracy. *J. Fluid Mech.* **199**, 471–494 (referred to herein as SG (1989)).

Tadjbakhsh, I. & Keller, J. B. 1960 Standing surface waves of finite amplitude. *J. Fluid Mech.* **8**, 442–451.

Umeki, M. 1989 Nonlinear dynamics and chaos in Faraday resonance. *J. Japan Soc. Fluid Mech.* **8**, 157–164 (in Japanese).

Umeki, M. & Kambe, T. 1989 Nonlinear dynamics and chaos in parametrically excited surface waves. *J. Phys. Soc. Japan* **48**, 140–154.

Verma, G. H. & Keller, J. B. 1962 Three-dimensional standing surface waves of finite amplitude. *Phys. Fluids* **5**, 52–56.